Supporting Information

Electro-Driven Fibrous Soft Actuators Towards Flapping-Wing Control for Insect-Scale Robots

*Ruitong Song, Yangyang Fan, Wenhao Hou, Zhiming Hu, Banghan Liu, Kai Liu, Jiu-an Lv**

R. Song, B. Liu, K. Liu
School of Materials Science and Engineering
Zhejiang University
Hangzhou, Zhejiang Province 310058, China

R. Song, Y. Fan, W. Hou, Z. Hu, B. Liu, K. Liu, J.-a. Lv
Key Laboratory of 3D Micro/Nano Fabrication and Characterization of Zhejiang Province
School of Engineering
Westlake University
Hangzhou, Zhejiang Province 310030, China
E-mail: lvjiuan@westlake.edu.cn

R. Song, Y. Fan, W. Hou, Z. Hu, B. Liu, K. Liu, J.-a. Lv
Institute of Advanced Technology
Westlake Institute for Advanced Study
Hangzhou, Zhejiang Province 310030, China

Supplementary Text S1.

Calculation methods of actuation parameters

$$\text{Actuation strain } (\%) = \frac{l_0 - l_t}{l_0} \times 100\%$$

where l_0 is the initial length of electro-driven LCE fibrous actuators and l_t is the length that the LCE fiber contracted along the longitudinal direction when powered on. l_0 and l_t were obtained from photos or videos by the software Kinovea.

$$\text{Strain rate } (\%/s) = \frac{d(\frac{l_0 - l_t}{l_0})}{dt}$$

The actuation strain rate was obtained by differentiating the actuation strain with respect to time.

$$\text{Power density } (W\,kg^{-1}) = \frac{P}{m_{LCE}} = \frac{W}{m_{LCE} \cdot t_{ac}} = \frac{m_{load} \cdot g \cdot (l_0 - l_t)}{m_{LCE} \cdot t_{ac}}$$

$$\text{Work density } (KJ\,m^{-3}) = \frac{W}{V_{LCE}} = \frac{m_{load} \cdot g \cdot (l_0 - l_t)}{V_{LCE}}$$

Mass power density and volume work density were calculated to facilitate comparison with other tasks, where P and W are the output power and work electro-driven LCE fibrous actuators during actuation, respectively. m_{LCE} and V_{LCE} is the mass and volume of LCE fibers, respectively. t_{ac} is the time of actuation response to power-on stimuli. m_{load} is the total mass of the loads and g is the acceleration of gravity.

Unless otherwise stated, electro-driven LCE fibrous actuators used to test actuation parameters have a length of 2 cm, a diameter of about 90 μm, and a mass of 0.13 mg.

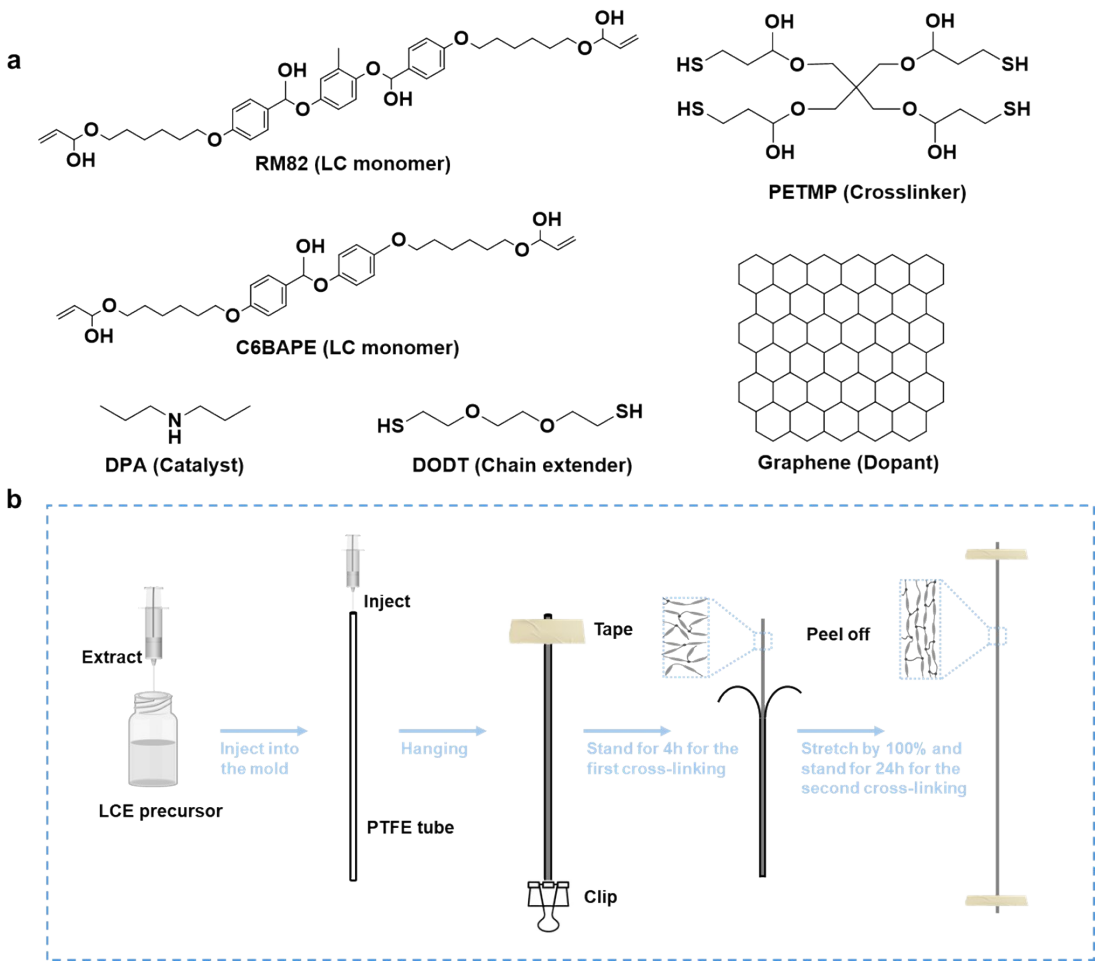

Figure S1. a) Materials for preparing LCE fibers. b) The process of preparing LCE fibers.

RM82 (1 g) and C6BAPE (0.409 g) were used as LC monomers, with a molar ratio of 2:1. DODT was used as a chain extender and PETMP as a crosslinking agent, with a molar ratio of 1:2, 1:1, 2:1, 4:1, and 6:1, respectively. The molar ratio of alkene to thiol was 1:1. Graphene (2 wt%, 0.037 g) was added to enhance the mechanical properties of LCE fibers. 3%wt DPA was added as a catalyst. Dissolve all the above materials in 5 mL of chloroform to get the LCE precursor, which was dispersed evenly by ultrasonics and then injected into polytetrafluoroethylene (PTFE) tubes with different diameters to get LCE fibers with different diameters. The tubes were placed for 4 hours and were peeled off to get the initially cross-linked LCE fibers. Then the fibers were stretched by 100% and placed for two days to carry out the second cross-linking and obtain the monodomain LCE fibers finally.

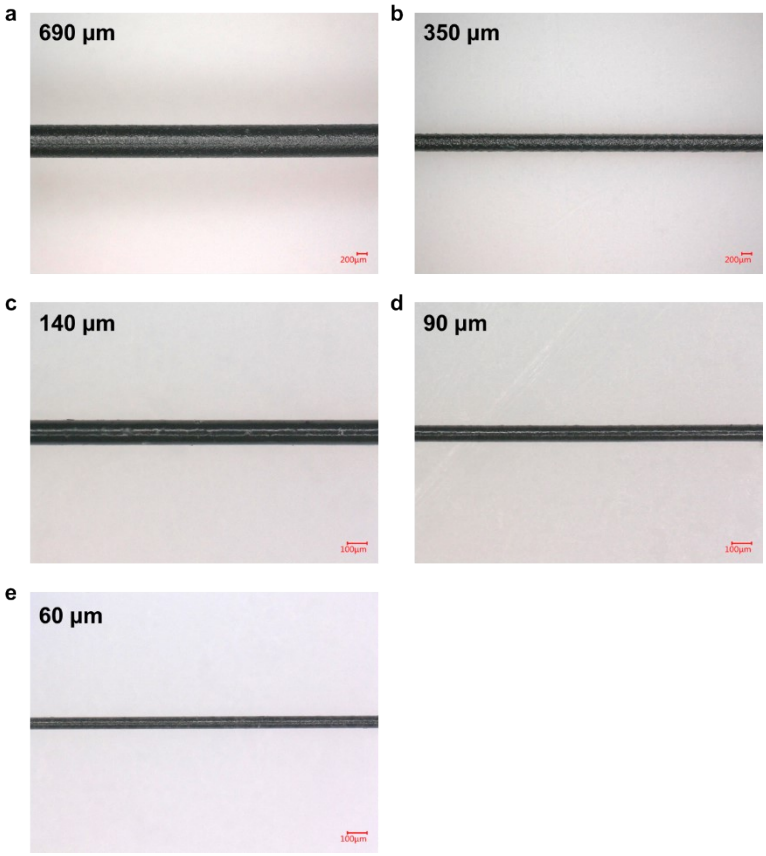

Figure S2. LCE fibers with different diameters. The photos were recorded by a super-resolution digital microscope (Keyence, VHX-1000C).

Table S1. The diameters of the molds required for LCE fibers of different diameters.

Tube diameter /μm	**LCE fiber diameter /μm**
800	690
500	350
300	140
200	90
150	60

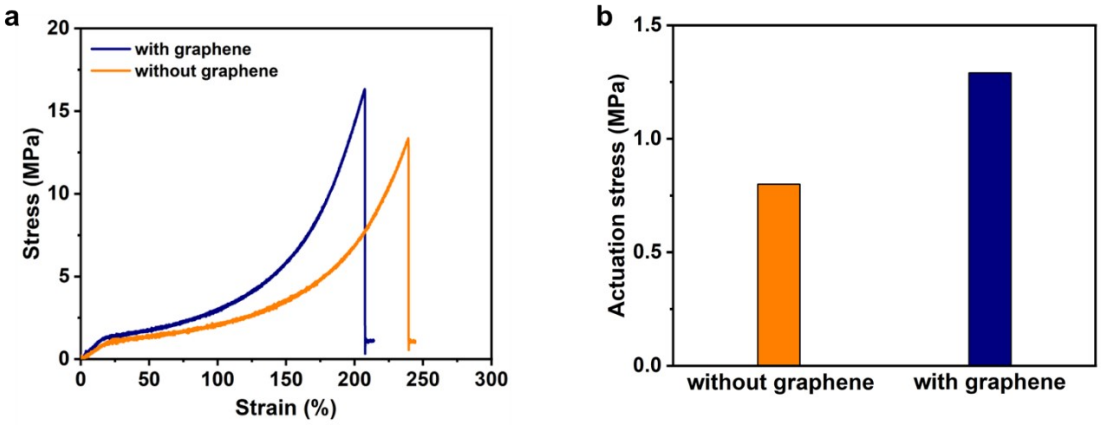

Figure S3. a) Stress-strain curve of LCE fibers doped with (blue line) or without (orange line) graphene. b) Actuation stress of LCE fibers doped with (blue line) or without (orange line) graphene.

Doping an appropriate amount of graphene can not only enhance the mechanical robustness of LCE fibers but also facilitate better actuation performance.[1,2] The LCE fibers doped with 2% graphene show a strength, strain, Young's modulus, and actuation stress of 16.5 MPa, 207.3%, 8.7 MPa, and 1.29 MPa, respectively, while those of LCE fibers without graphene are 13.5 MPa, 239.8%, 2.1 MPa, and 0.80 MPa. The increasing strength and modulus are beneficial to amplify the output force of actuated LCE fibers.

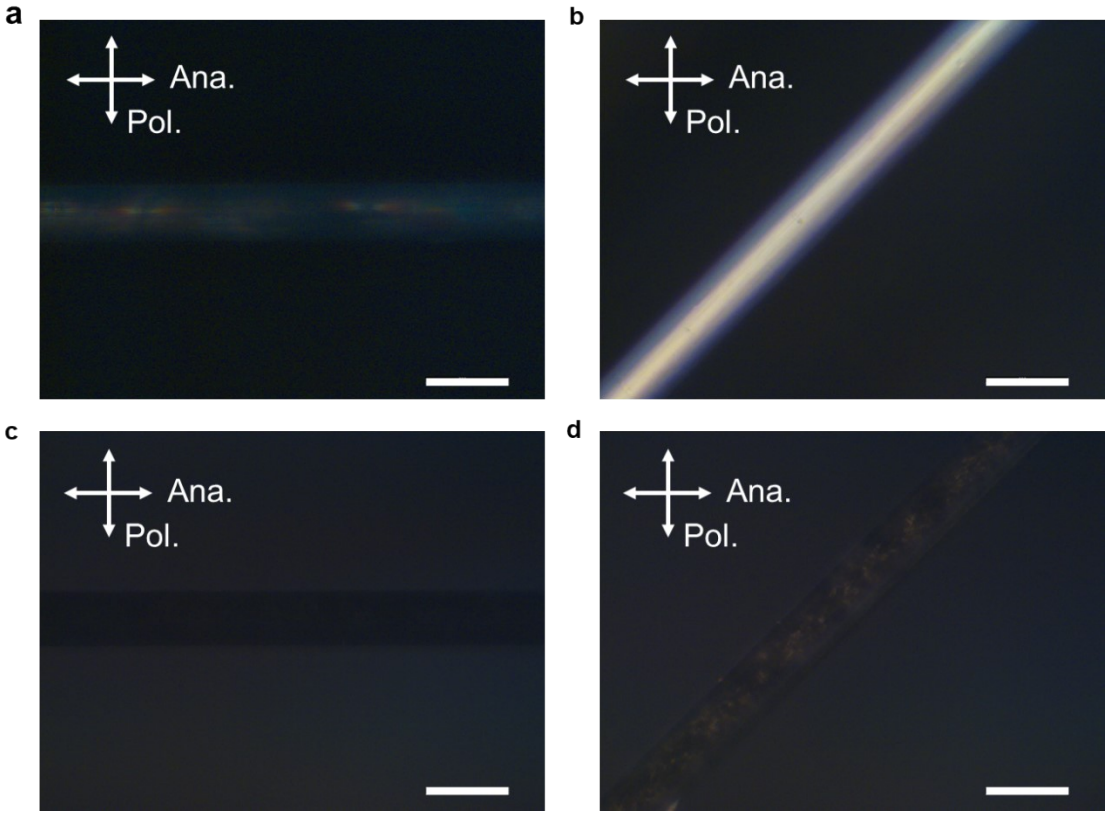

Figure S4. a) and b) Reflection microscopy images of LCE fibers without graphene at two different angles with respect to the analyzer and polarizer. c) and d) Reflection microscopy images of LCE fibers with graphene at two different angles with respect to the analyzer and polarizer. (scale bar: 200 μm). The mesogen alignment of the monodomain LCE fibers was confirmed by the polarizing microscope (POM, Leica DM2700 P).

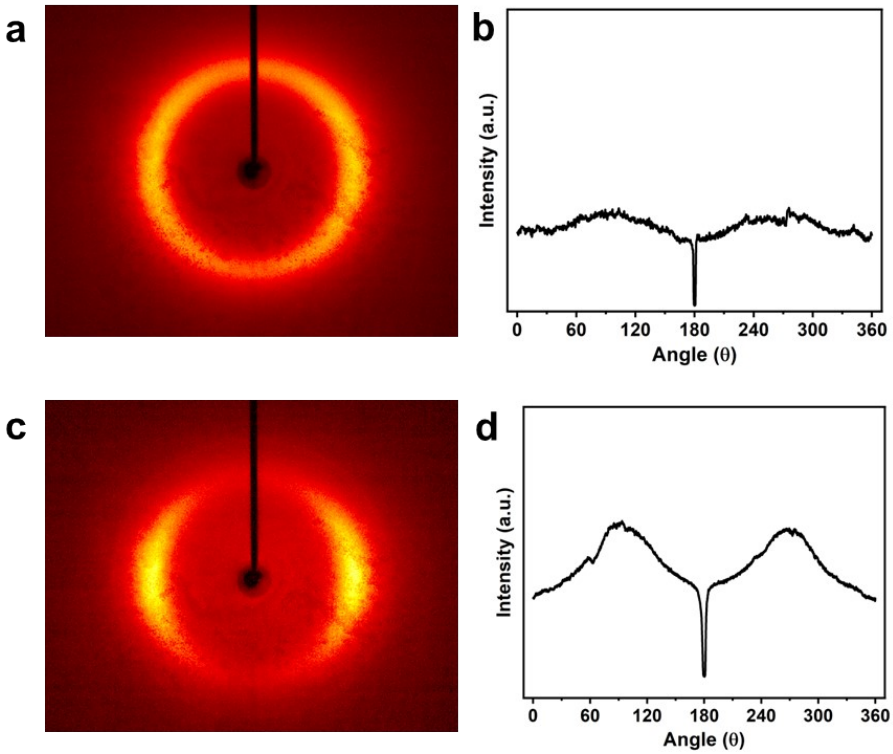

Figure S5. a) 2D Wide-angle X-ray diffraction patterns and b) order parameter of LCE fiber before alignment. c) 2D Wide-angle X-ray diffraction patterns and d) order parameter of LCE fiber after alignment. 2D Wide-angle X-ray diffraction patterns were obtained by using a Bruker D8 Venture diffractometer.

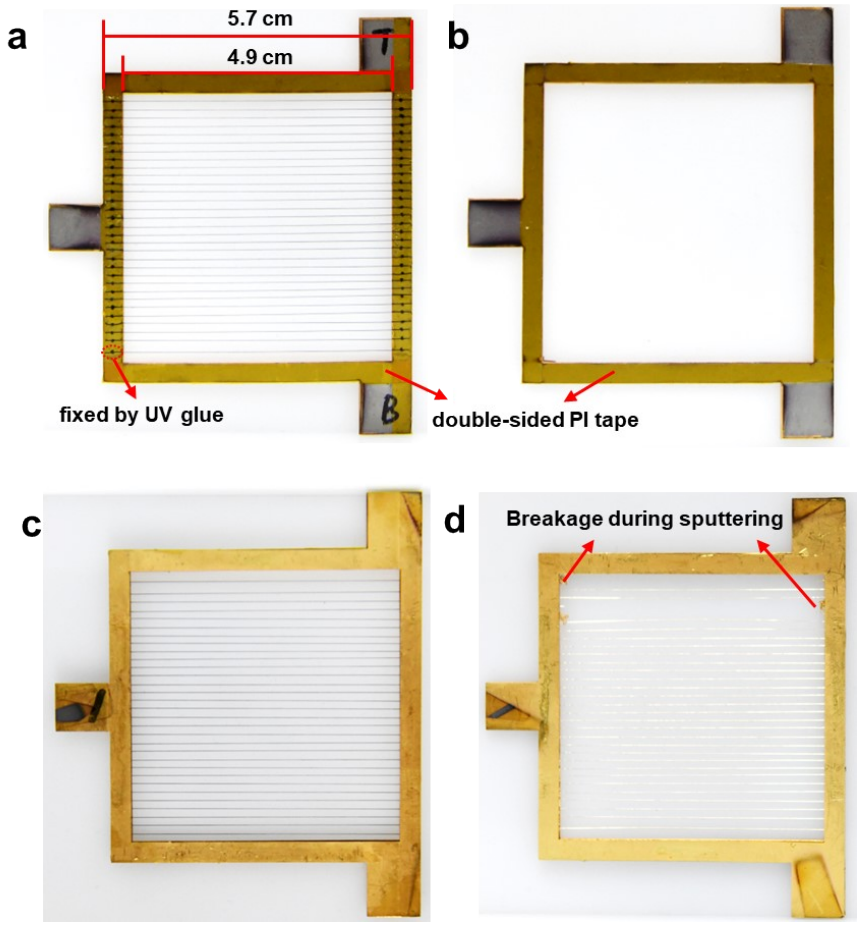

Figure S6. a) Pre-stretch LCE fibers on the bottom stainless-steel mold. b) Upper stainless-steel mold. c) Assembled the mold with double-sided PI tape and then clamped it with clips for better bonding. d) Mold after sputtering Au. Due to internal stress, some fibers would break during sputtering.

The size of the mold (thickness: 1 mm) was designed based on the size of the sample stage and the baffle of the magnetron sputtering.

Sputtering process of the Au coating: A base pressure of 4×10^{-5} mbar was vacuumed during the sputtering process. The working gas (Ar) pressure was around 3.3×10^{-3} mbar during sputtering. A thin coating of Cr (thickness: ~5 nm) was first deposited as an adhesion coating onto the LCE fiber, then Au (thickness: ~150 nm) was deposited on Cr without breaking the vacuum. Then broke the vacuum, flipped the mold, and repeated the sputter process to ensure that the Au coating was wrapped around the fibers.

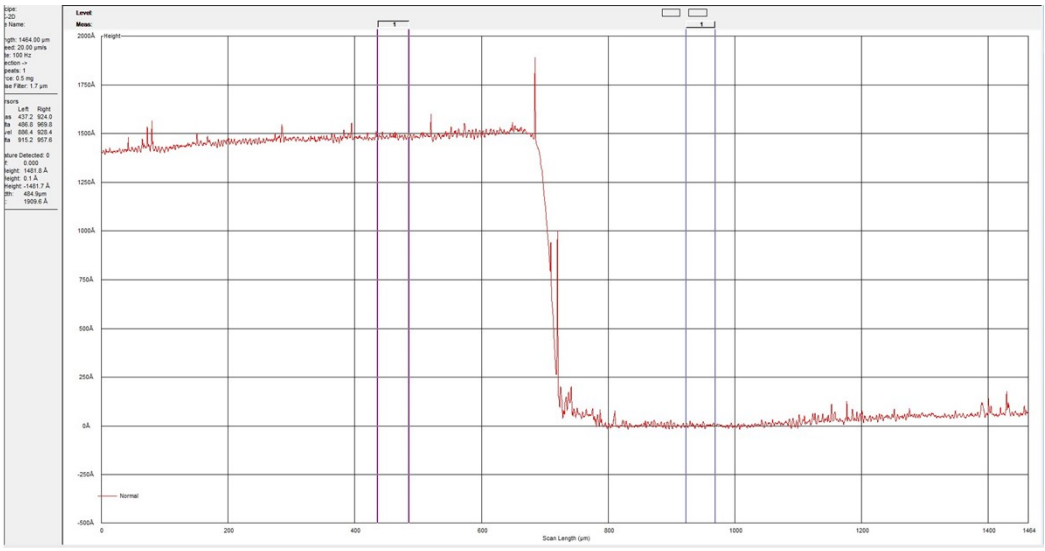

Figure S7. Thickness of Au coating, about 150 nm, tested by Stylus Profiler (WCMNF-2019-C003, KLA-Tencor).

The thickness was tested by sputtering Au on a glass slide with the same parameters as sputtering LCE fibers. Part of the slide glass was covered by adhering PI tape. After sputtering, the tape was removed to form a thickness difference with the uncovered part to test.

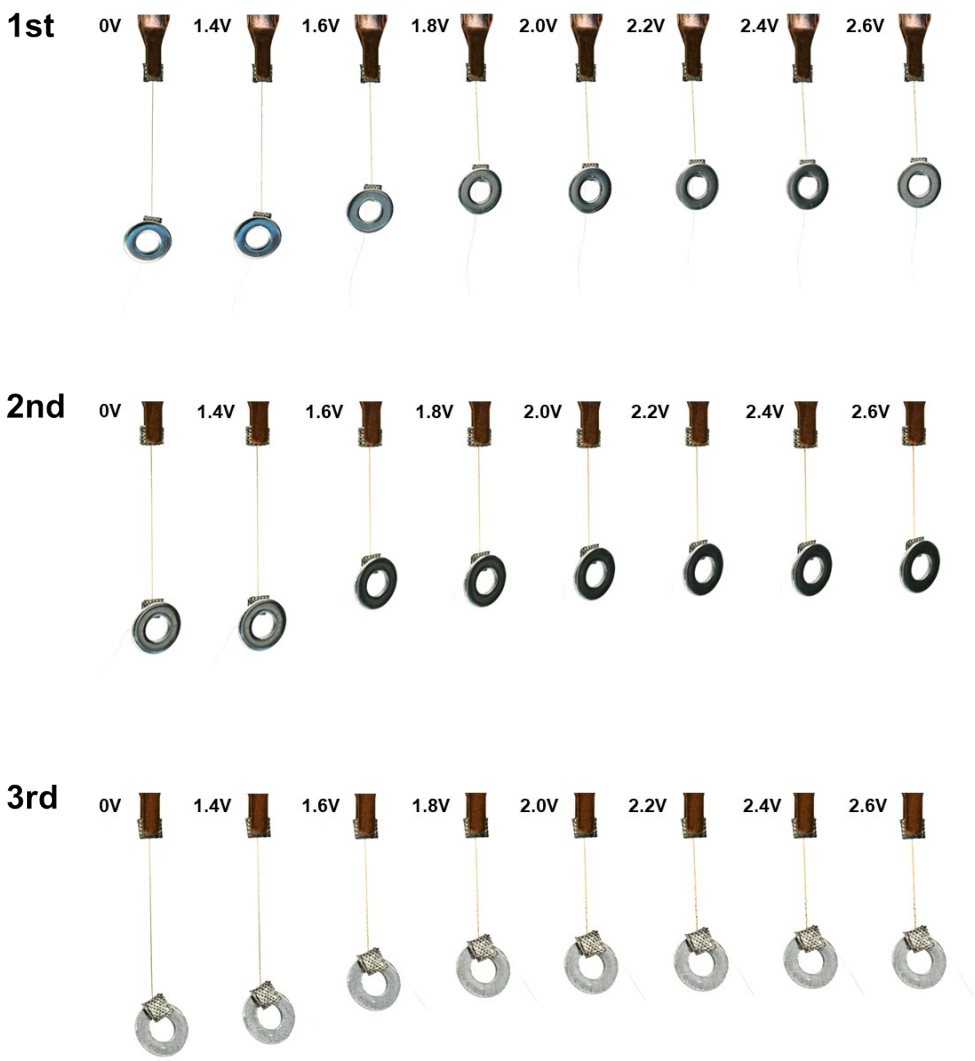

Figure S8. The actuating strain of electro-driven LCE fibrous actuators under different voltages. The load was 74 mg.

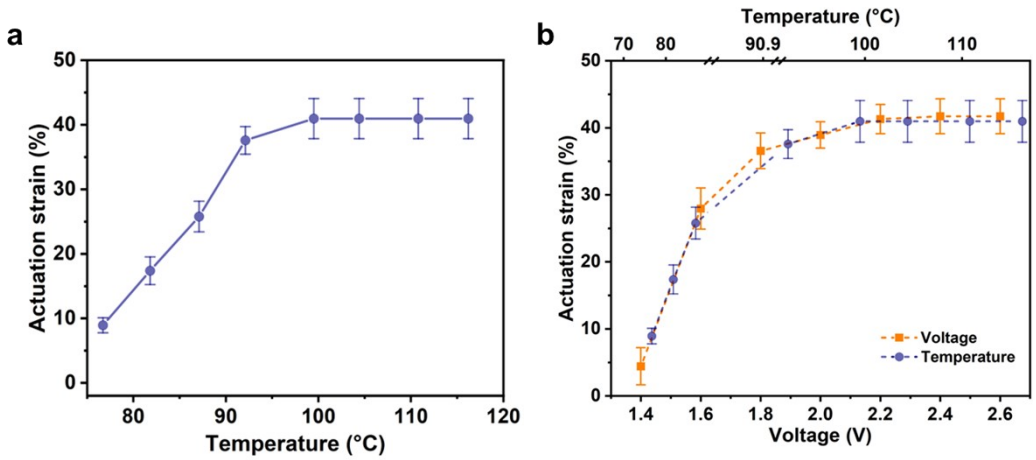

Figure S9. a) The actuating strain of electro-driven LCE fibrous actuators varied with temperature. b) The actuating strain of electro-driven LCE fibrous actuators changed with voltage and temperature. The heating temperature corresponding to different voltages could be obtained.

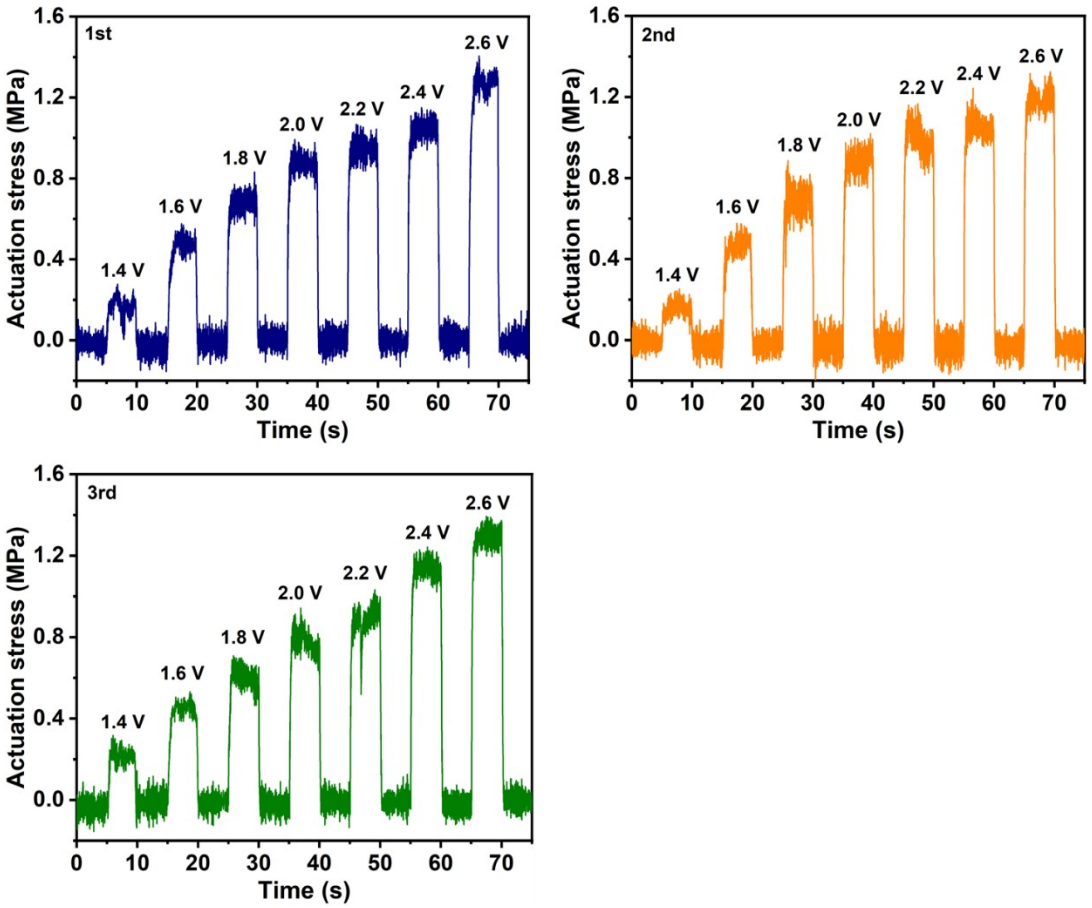

Figure S10. The actuation stress of electro-driven LCE fibrous actuators under different voltages, tested using a tensile testing machine and an electrochemical workstation together.

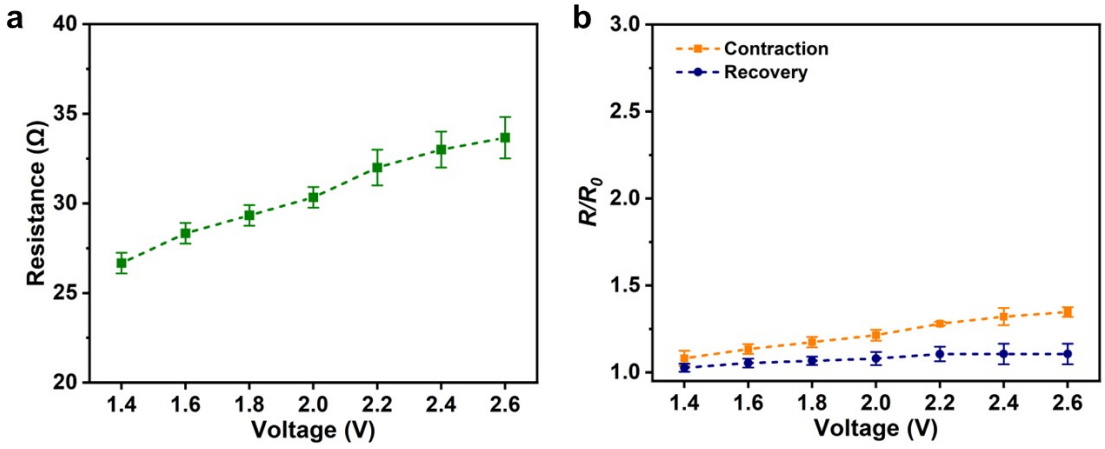

Figure S11. a) The resistance of Au coating changed with voltage. b) The relative resistance changes of Au coating varied with voltage.

The resistance was calculated by dividing the voltage by the current by applying a voltage of 0.5 V for 5 s on Au-coated LCE fibers through *i-t* mode of CHI760e.

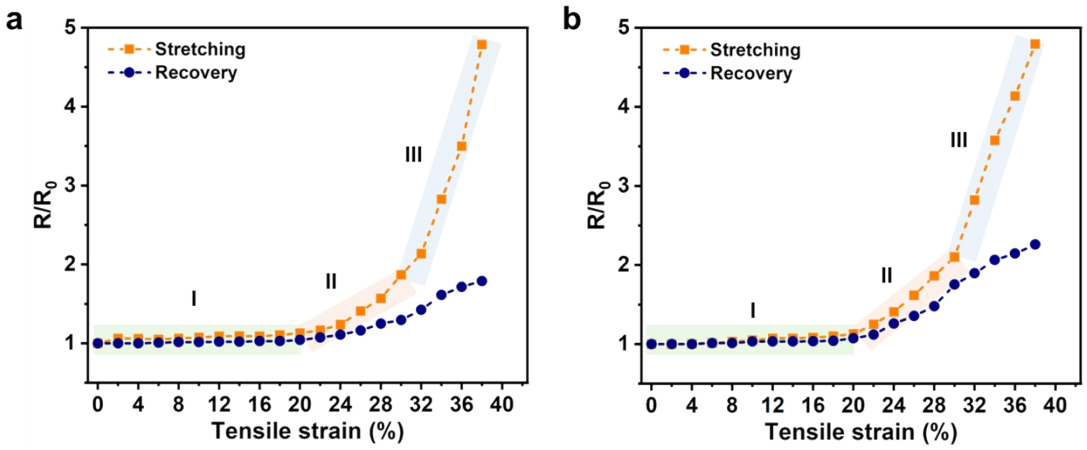

Figure S12. Two other tests that showed R/R_0 changed with tensile strain, tested by using a tensile testing machine and an electrochemical workstation together. The resistance was calculated by dividing the voltage by the current by applying a voltage of 0.5 V for 5 s on Au-coated LCE fibers through *i-t* mode of CHI760e.

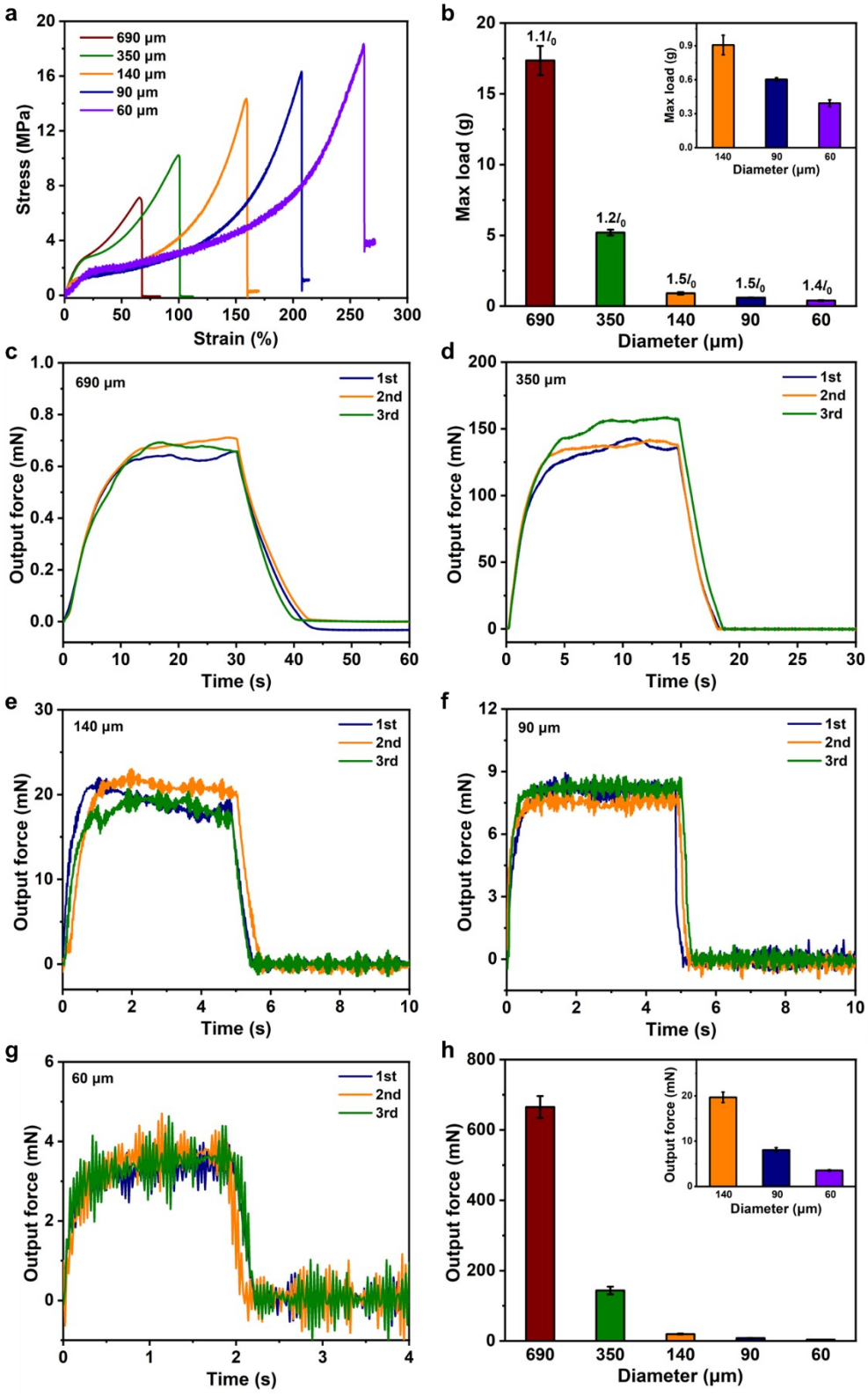

Figure S13.a) Strain-stress curve, b) the max actuatable load, and c)-h) output force of LCE fibers with different diameters. The output forces were tested by applying a voltage of 2.2 V for 30 s, 15 s, 5 s, 5 s, and 2 s for LCE fibers with a diameter of 690 μm, 350 μm, 140 μm, 90 μm, and 60 μm, respectively.

Table S2. Properties of LCE fibers with different diameters.

Diameter /μm	Tensile stress /MPa	Elongation at break/%	Young's modulus /MPa	Output force/mN	Safe pre-stretch	Max actuatable load (g)	Max actuation strain rate/% s^{-1}
690	7.2	66.8	21.7	665.2	1.1	17.35	15.5
350	10.3	99.8	20.4	145.0	1.3	5.23	62.0
140	14.4	159.1	13.6	21.6	1.5	0.91	89.1
90	16.5	207.3	8.7	8.3	1.5	0.60	140.5
60	18.5	261.9	8.8	3.5	1.4	0.41	157.0

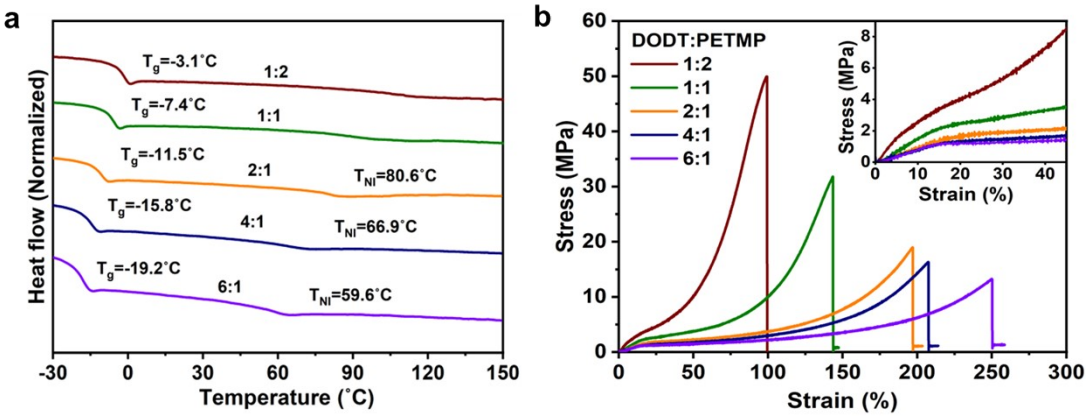

Figure S14. a) DSC and b) Stress-strain curve of LCE fibers with different molar ratios of DODT and PETMP.

Table S3. Properties of LCE fibers with different ratios of DODT and PETMP.

DODT: PETMP	T_g/°C	T_{NI}/°C	Tensile stress /MPa	Elongation at break/%	Young's modulus /MPa	Actuation stress/MPa	Safe pre-stretch	Max actuatable mass (g)
1:2	-3.1	-	50.3	99.5	37.5	3.36	1.1	0.51
1:1	-7.4	-	31.9	143.4	18.3	2.72	1.1	0.39
2:1	-11.5	80.6	19.1	196.7	9.4	1.40	1.3	0.49
4:1	-15.8	66.9	16.5	207.3	8.7	1.29	1.5	0.60
6:1	-19.2	59.6	13.4	250.3	8.5	0.74	1.6	0.42

T_g: glass transition temperature. T_{NI}: phase transition temperature.

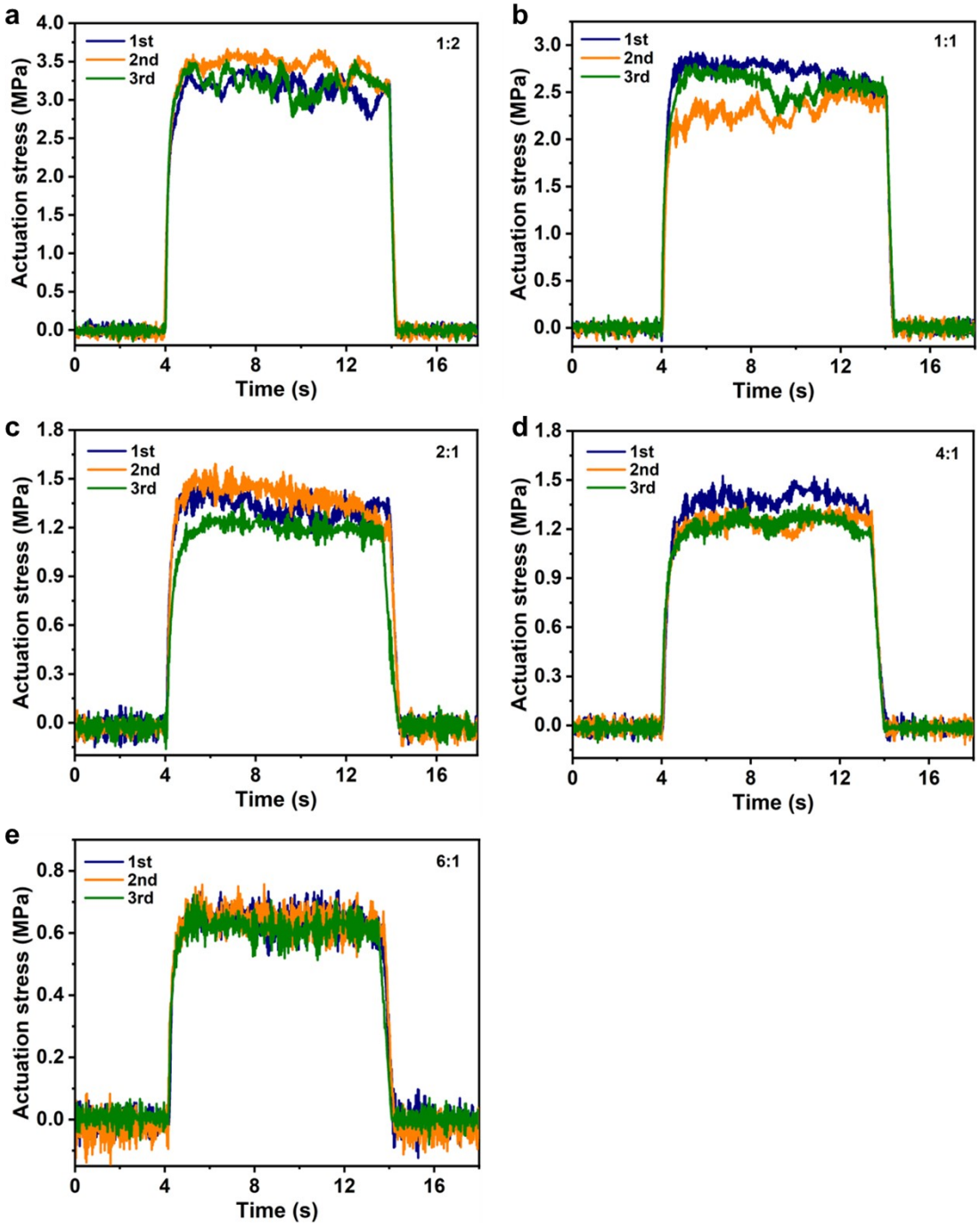

Figure S15. a)-e) Actuation stress of electro-driven LCE fibrous actuators with different molar ratios of DODT and PETMP under a voltage of 2.2 V.

Table S4. The maximum pre-stretch proportion of different molar ratios of DODT and PETMP under different circumstances.

DODT: PETMP	l/l_0										
	1.1	1.2	1.3	1.4	1.5	1.6	1.7	1.9	2.1	2.3	2.5
1:2		Break when sputter				Break when pre-stretch					
1:1											
2:1											
4:1		Safe									
6:1											

l : the length after stretching
l_0 : the original length

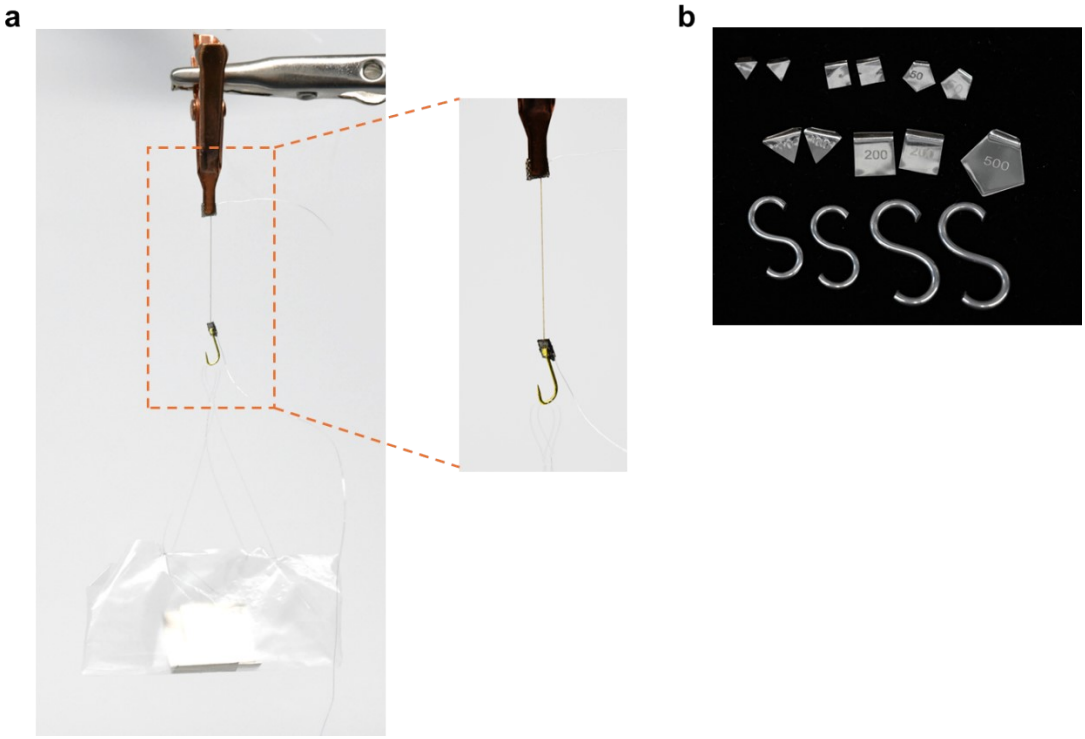

Figure S16. a) The structure used to measure the actuatable mass. The total mass of the fishhook, fishing line, and the plastic pocket for holding the weights is 0.02 g. The fishhook is fixed on the electrode by UV glue. b) Weights used for testing, from 10 mg to 2 g.

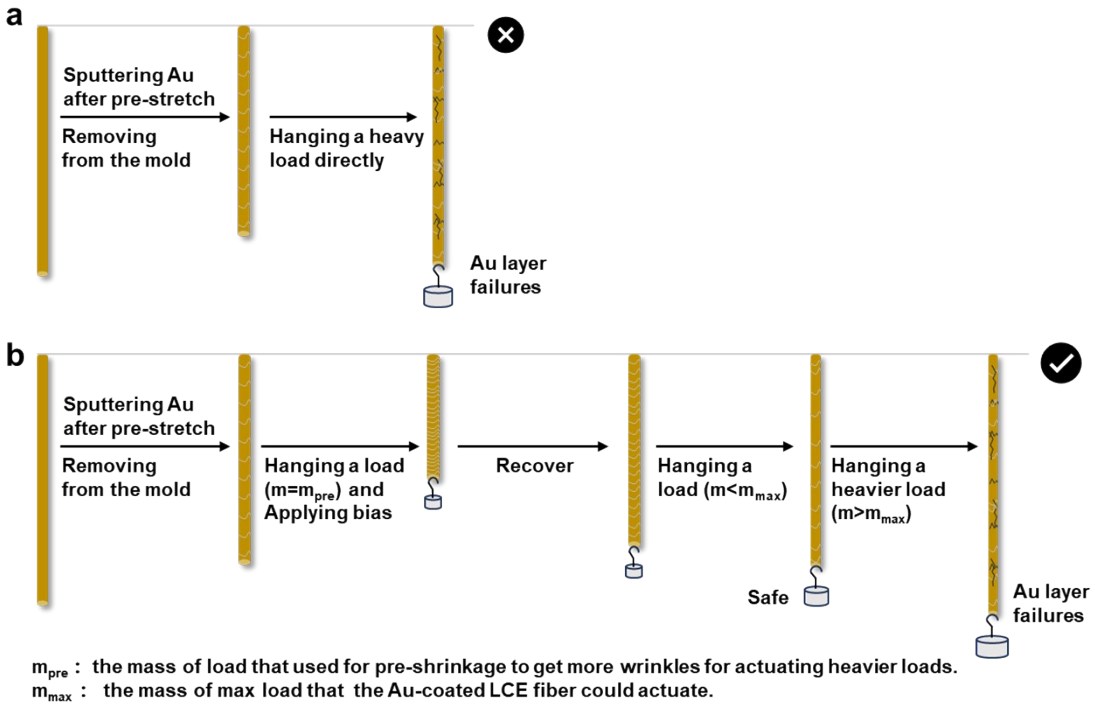

Figure S17. a) The influence of LCE fiber actuation on the Au coating without pre-shrinking. b) The influence of LCE fiber actuation on the Au coating with pre-shrinking.

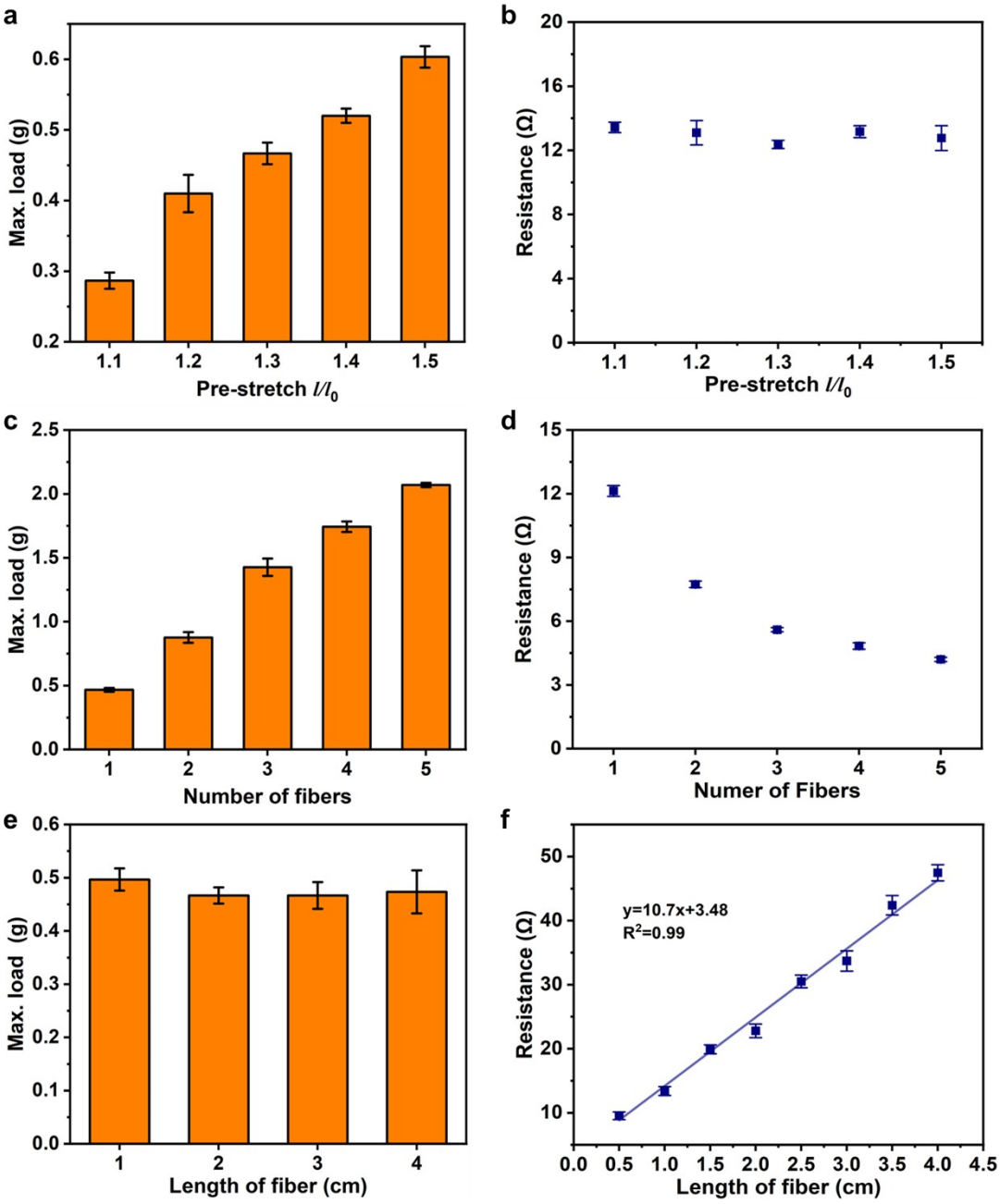

Figure S18. a) The maximum electro-driven load (*Max. load*) and b) the resistance (*R*) of Au-coated LCE fibers with different pre-stretch proportions (number: 1, length: 1 cm). c) Max actuatable loads and d) resistances of Au-coated LCE fibers with different numbers (pre-stretch: 1.3x, length: 1 cm). e) Max actuatable loads and f) resistances of Au-coated LCE fibers with different lengths (pre-stretch: 1.3x, number: 1).

1Hz

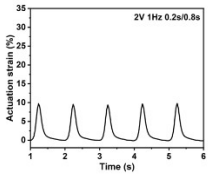

9.6%

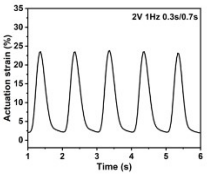

21.4%

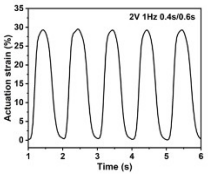

29.1%

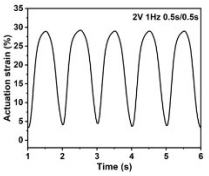

25.3%

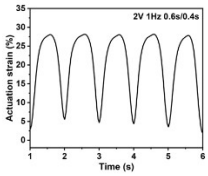

23.0%

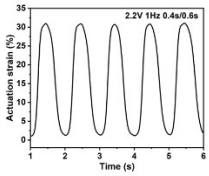

29.6%

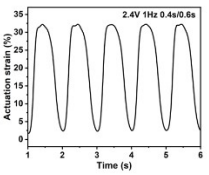

30%

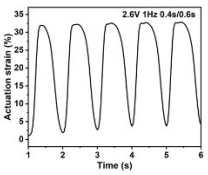

30.1%

2Hz

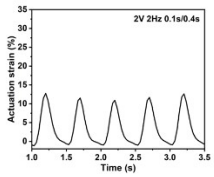

12.2%

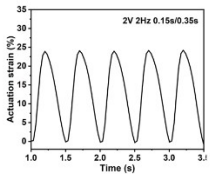

24.4%

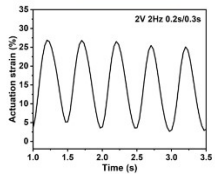

22.1%

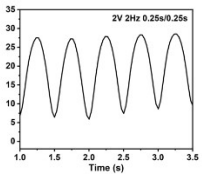

21.1%

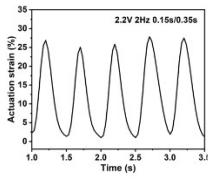

25.2%

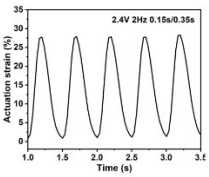

27.0%

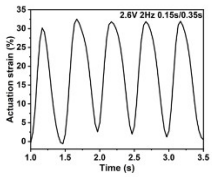

30.0%

4Hz

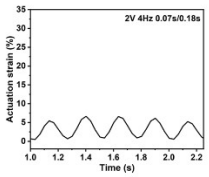

6.0%

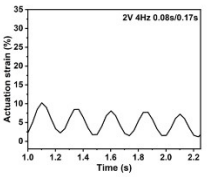

9.6%

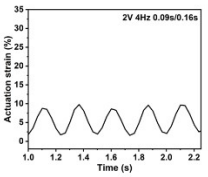

8.3%

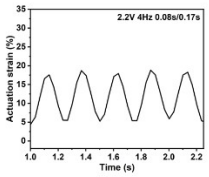

12.8%

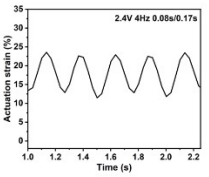

11.5%

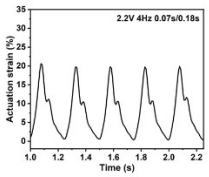

19.3%

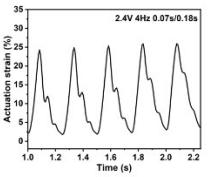

23.4%

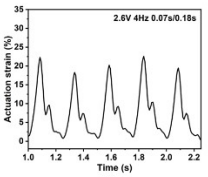

19.5%

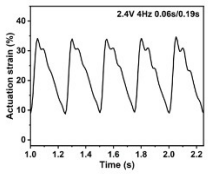

25.7%

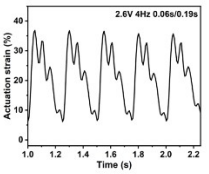

31.0%

6Hz

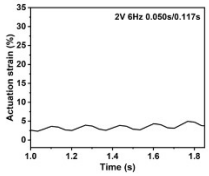

1.5%

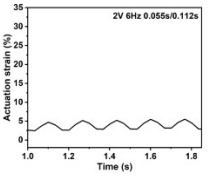

2.8%

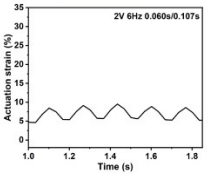

4.0%

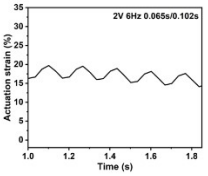

3.2%

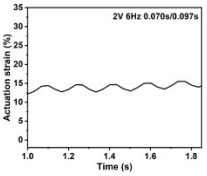

2.1%

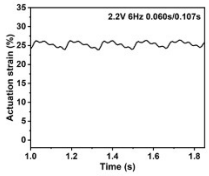

2.5%

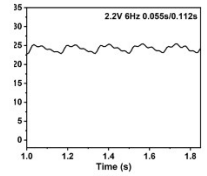

2.8%

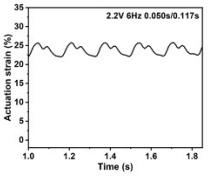

3.9%

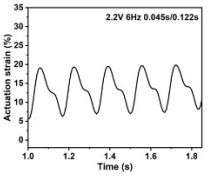

12.8%

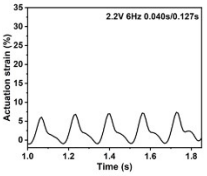

8.2%

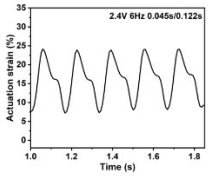

16.9%

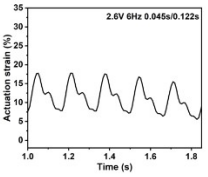

10.3%

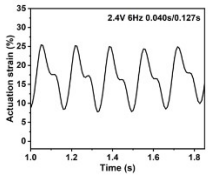

17.6%

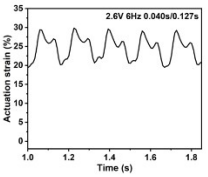

10.0%

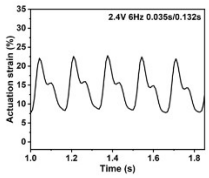

14.5%

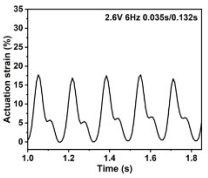

17.3%

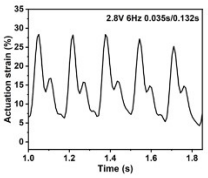

22.1%

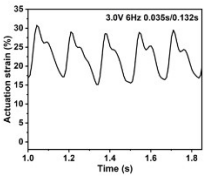

13.5%

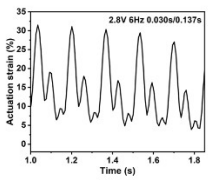

23.6%

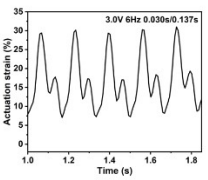

22.4%

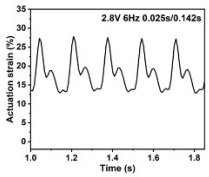

14.9%

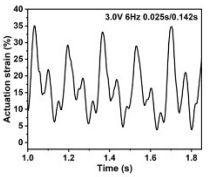

30.0%

8Hz

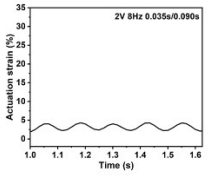

2.1%

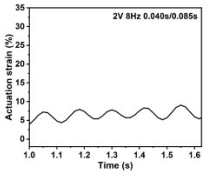

3.6%

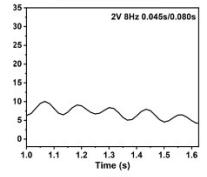

3.1%

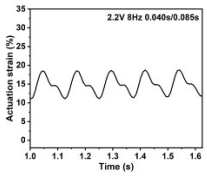

8.0%

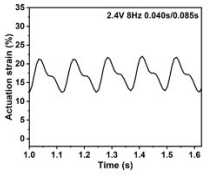

9.2%

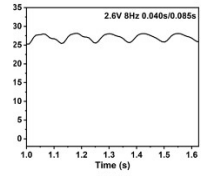

2.9%

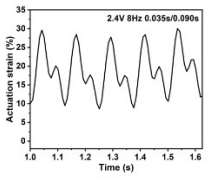

19.2%

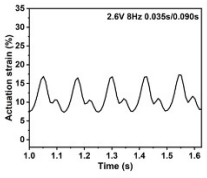

9.5%

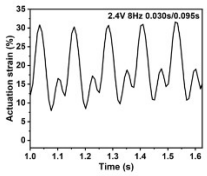

22.6%

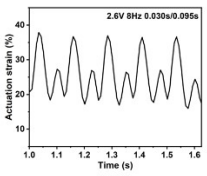

19.0%

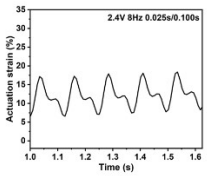

11.2%

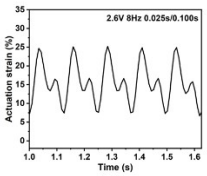

17.8%

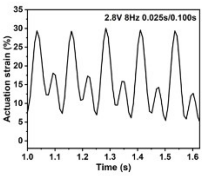

23.4%

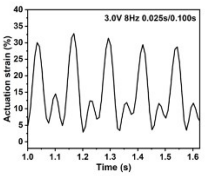

28.2%

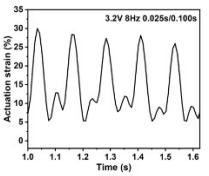

22.7%

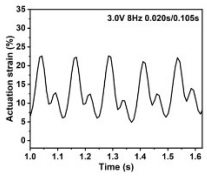

16.4%

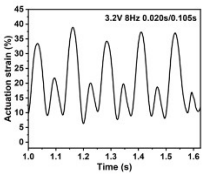

30.2%

10Hz

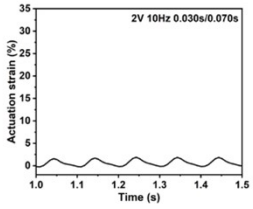

2.4%

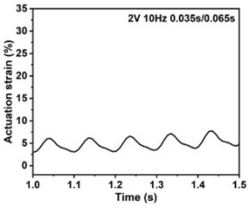

3.5%

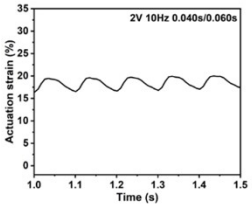

3.3%

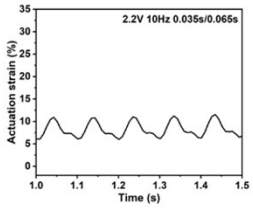

5.3%

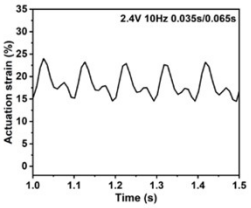

8.3%

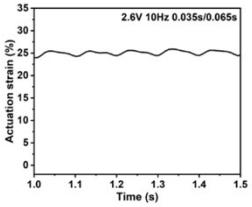

1.3%

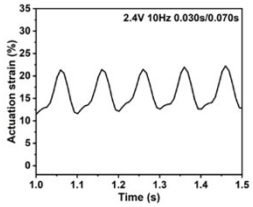

10.0%

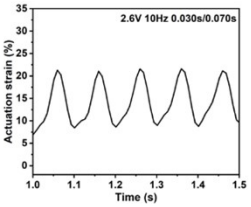

13.3%

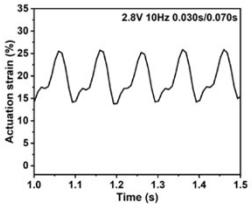

11.6%

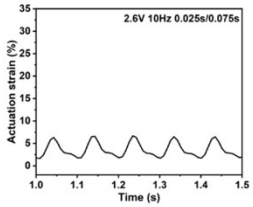

4.9%

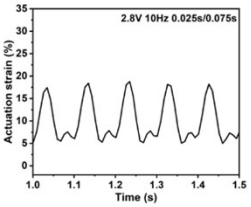

12.6%

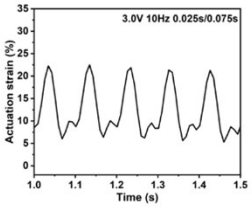

14.2%

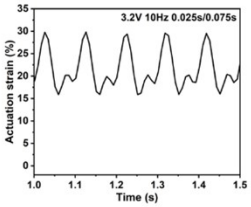

11.6%

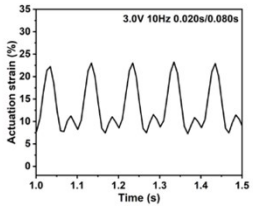

14.8%

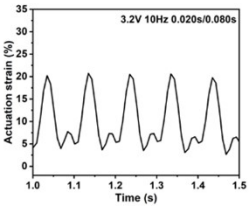

16.2%

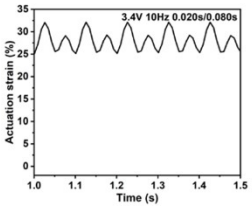

7.2%

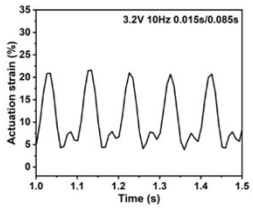

17.5%

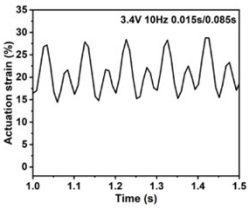

12.0%

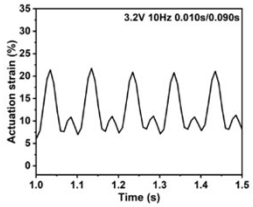

15.7%

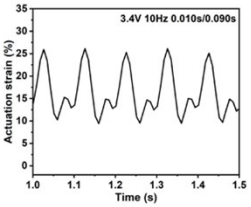

16.3%

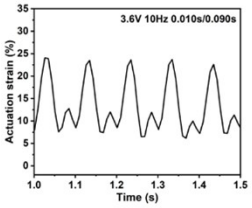

16.5%

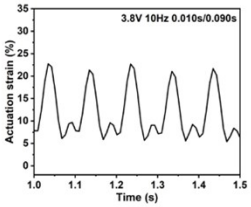

16.0%

20Hz

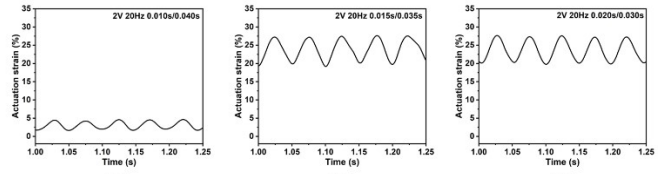

2.5% 7.6% 7.3%

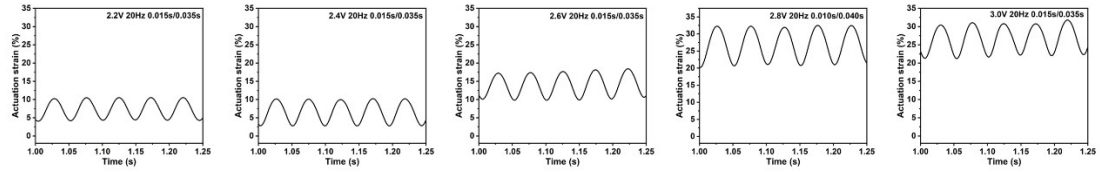

6.5% 7.6% 8.8% 9.4% 8.8%

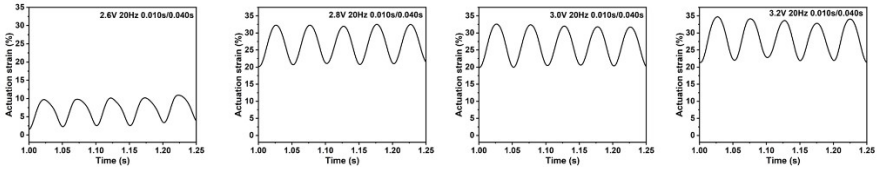

7.7% 12.4% 13.0% 12.6%

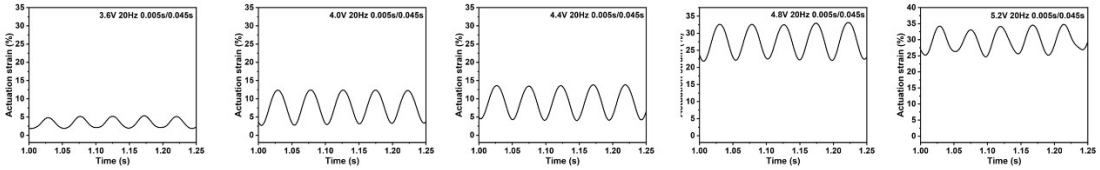

3.6% 9.8% 9.6% 10.7% 9.8%

30Hz

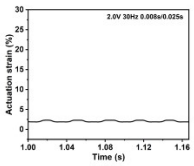

0.66%

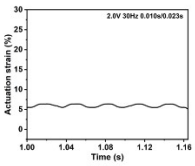

1.17%

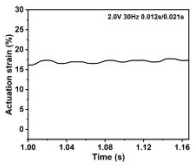

1.13%

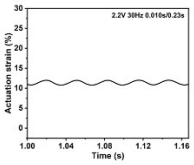

1.48%

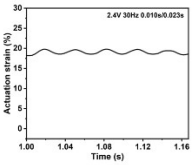

1.39%

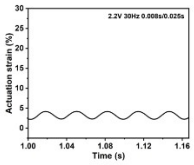

2.15%

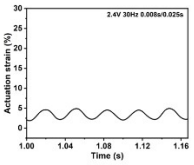

2.72%

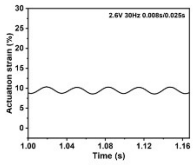

1.85%

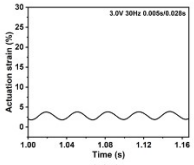

2.15%

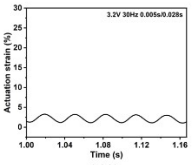

2.31%

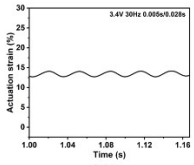

1.61%

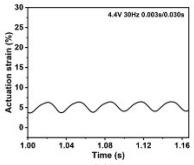

2.85%

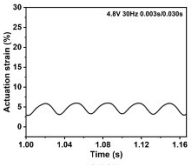

2.90%

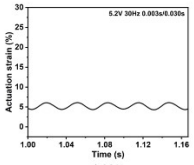

1.88%

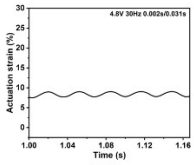

1.54%

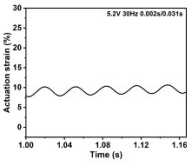

2.33%

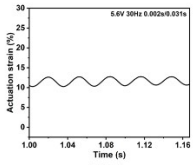

2.66%

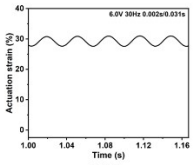

3.63%

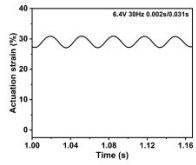

4.04%

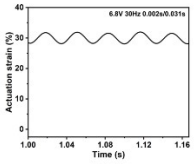

3.86%

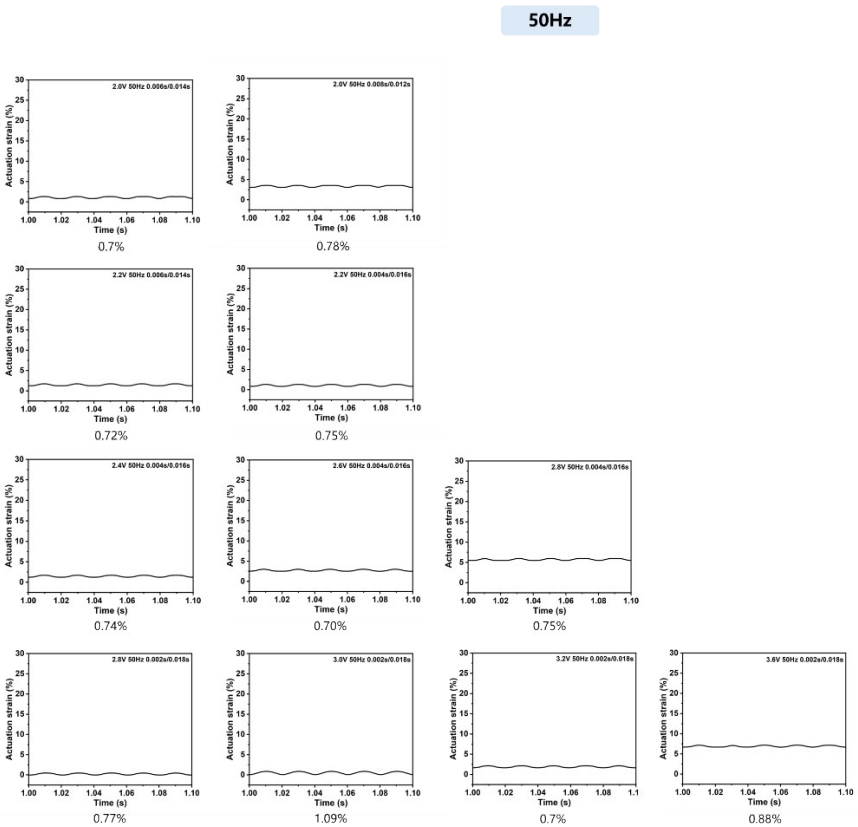

Figure S19. The actuation strain of electro-driven LCE fibrous actuators changes with voltage (V) and power-on time (t_{on}) at 1 Hz, 2 Hz, 4 Hz, 6 Hz, 8 Hz, 10 Hz, 20 Hz, 30 Hz, and 50 Hz.

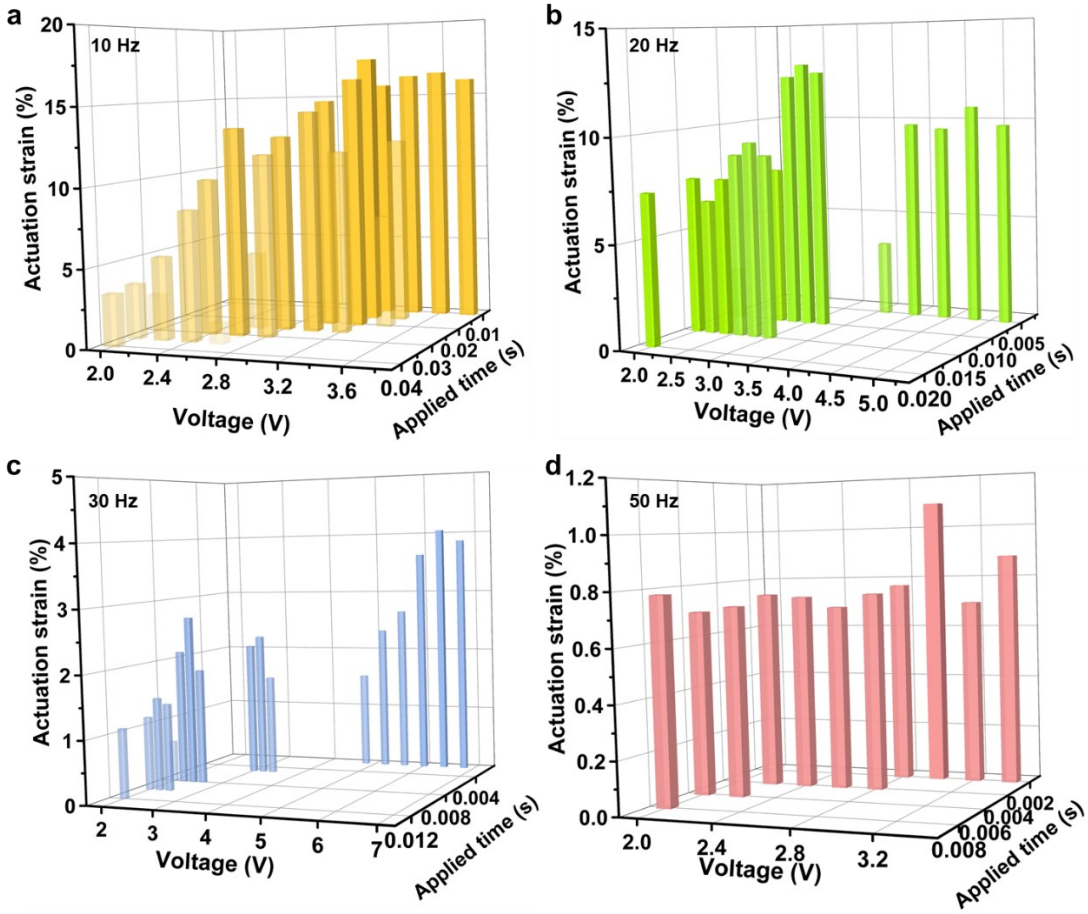

Figure S20. The actuation strain of electro-driven LCE fibrous actuators changes with V and t_{on} at a) 10 Hz, b) 20 Hz, c) 30 Hz, and d) 50 Hz.

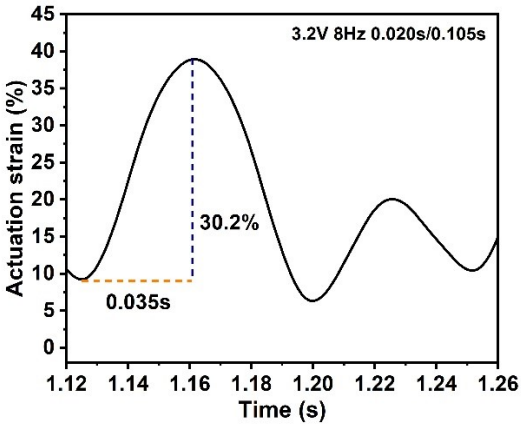

Figure S21. The actual actuation time (t_{ac}, 0.035 s) is longer than the power-on time (t_{on}, 0.020 s) due to heat accumulation.

4Hz

100mg

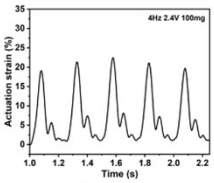

0.070s 20.8%

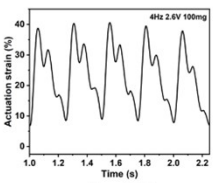

0.054s 32.1%

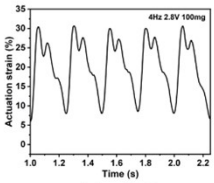

0.054s 22.0%

200mg

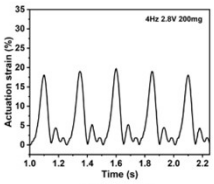

0.066s 17.4%

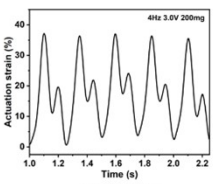

0.090s 34.4%

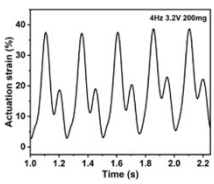

0.097s 34.7%

300mg

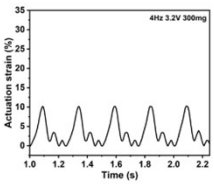

0.087s 10.5%

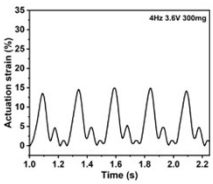

0.080s 14.9%

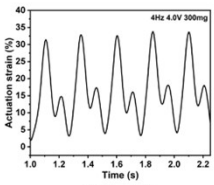

0.083s 31.0%

400mg

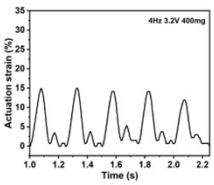

0.076s 15.5%

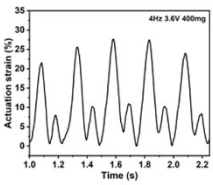

0.082s 26.4%

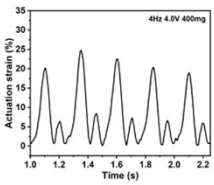

0.077s 22.4%

6Hz

100mg

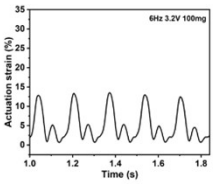

0.043s 11.1%

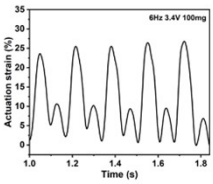

0.045s 26.5%

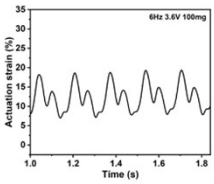

0.044s 10.4%

200mg

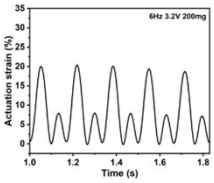

0.050s 20.1%

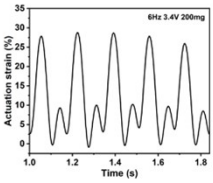

0.050s 26.8%

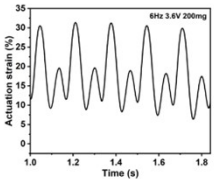

0.043s 20.6%

300mg

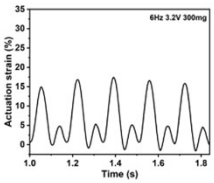

0.050s 17.0%

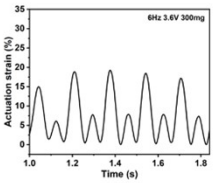

0.045s 19.0%

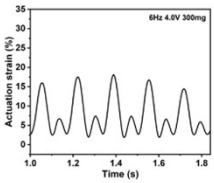

0.049s 15.7%

400mg

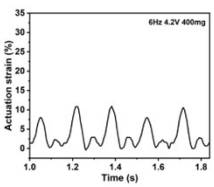

0.047s 9.5%

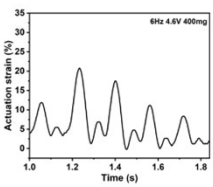

0.049s 14.5%

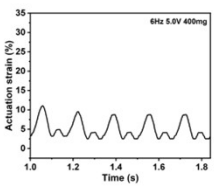

0.049s 8.1%

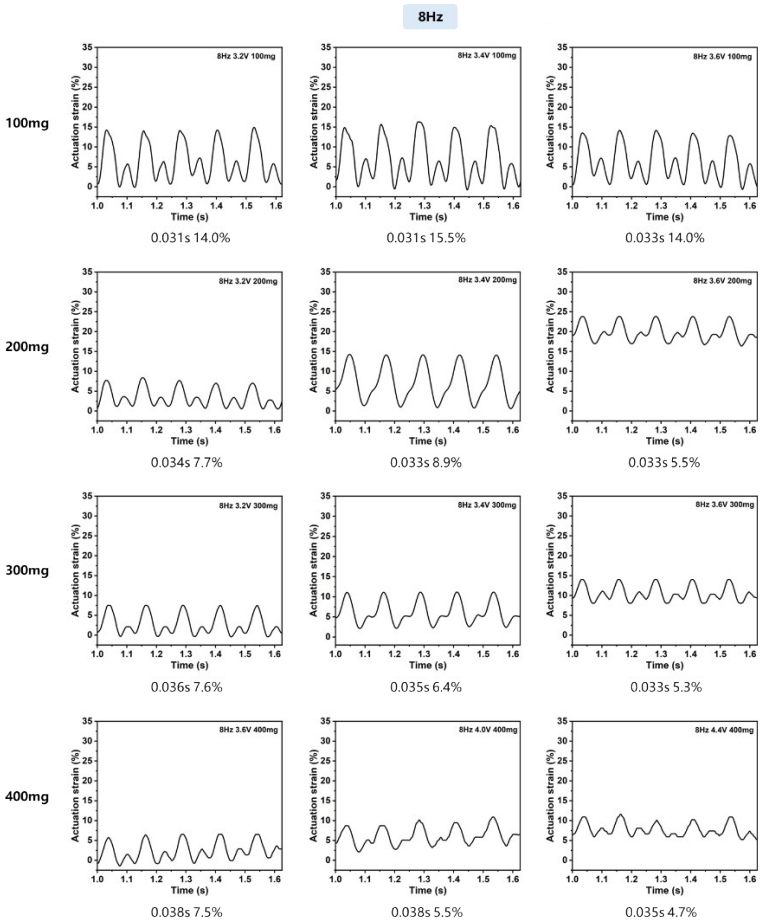

Figure S22. Actuation strain of electro-driven LCE fibrous actuators changes with V and m_{load} under 4 Hz, 6 Hz, and 8 Hz. The t_{on} of 4 Hz, 6 Hz, and 8 Hz are 0.060 s, 0.025 s, and 0.020 s, respectively. The device used in the test is shown in Figure S12. When calculating the power density, the m_{load} includes the masses of the weights and the device (fishhook, fishing line, and the plastic pocket for holding the weights, total mass 0.02 g).

For a fixed frequency, even if the t_{on} are the same, due to the different V and m_{load}, the resonant interactions between the electro-driven LCE fibers and the loads during the actuation process are different, so the t_{ac} also vary accordingly. The t_{ac} are obtained from the above figures and used to calculate the power density.

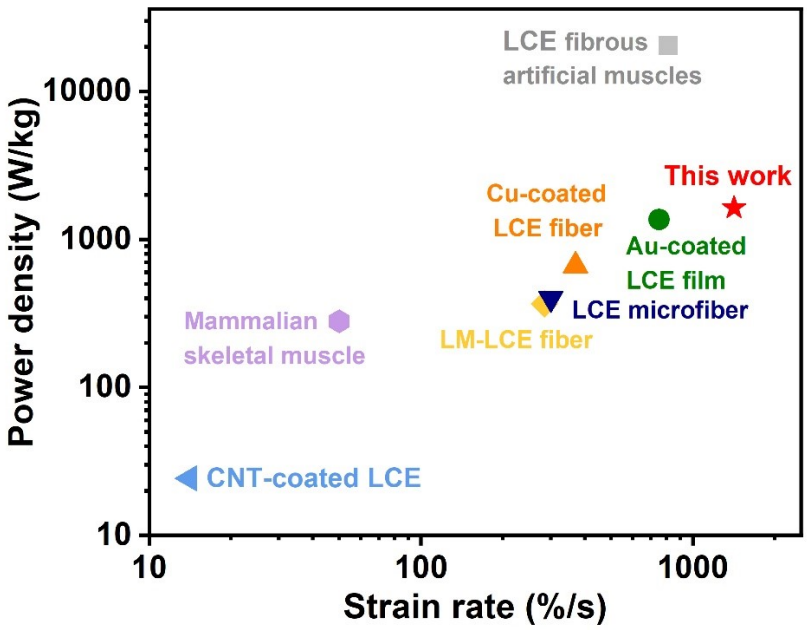

Figure S23. Ashby plot of power density versus actuation strain rate of actuators, which include Mammalian skeletal muscle,[3] CNT-coated LCE,[4] LM-LCE fiber,[5] LCE microfiber,[6] Cu-coated fiber,[7] Au-coated film,[8] and LCE fiberous artificial muscles.[2]

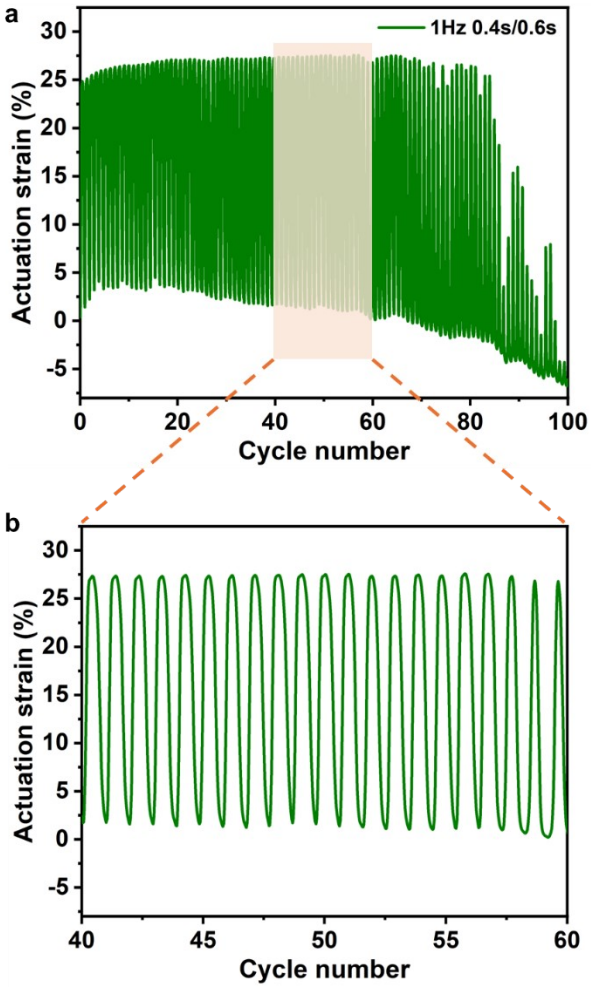

Figure S24. Durability of the electro-driven LCE fibrous actuators under cyclic actuation (V = 2.2 V, f = 1 Hz, t_{on} = 0.4 s, t_{off} = 0.6 s).

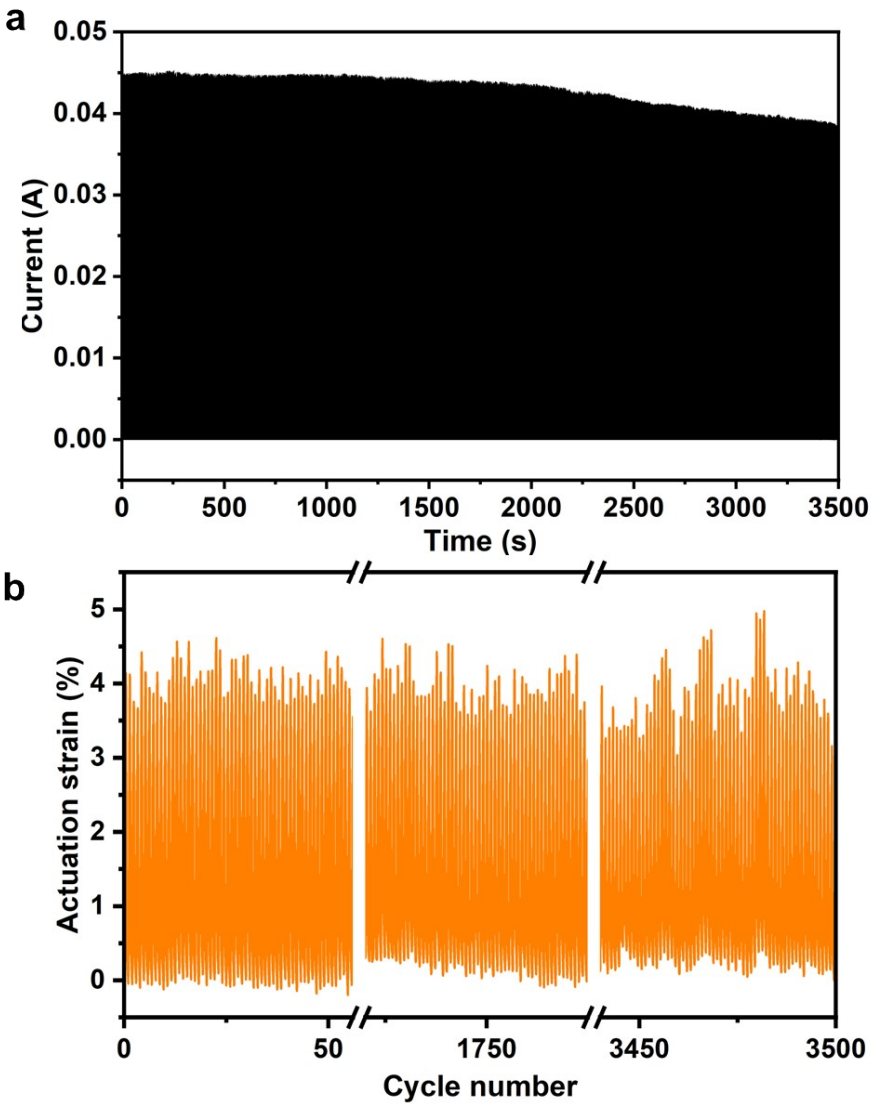

Figure S25. a) Current-time diagram of applying an electrical cyclic stimulus (V = 1.4 V, f = 1 Hz, t_{on} = 0.4 s, t_{off} = 0.6 s). The change in resistance (~31 Ω - ~36 Ω) before and after 3500 cycles can be obtained. b) Durability of the electro-driven LCE fibrous actuators under cyclic actuation (V = 1.4 V, f = 1 Hz, t_{on} = 0.4 s, t_{off} = 0.6 s).

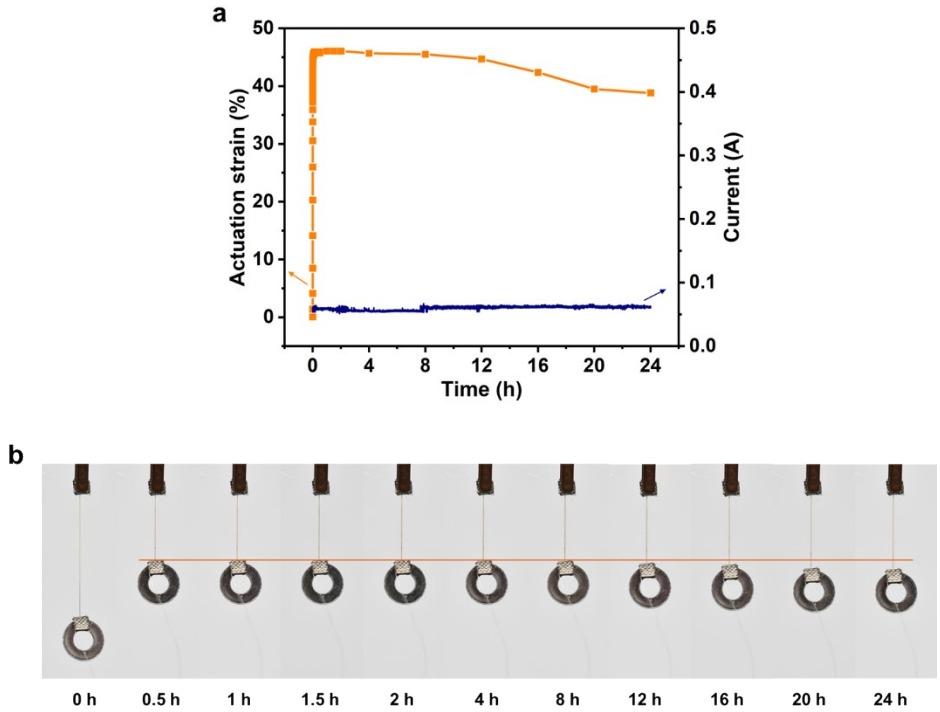

Figure S26. Creep behavior of the LCE fibrous actuator when actuated by electricity. a) Actuation strain changed with time when a continuous 2.2 V voltage was applied. b) Photos during the changing process.

Under prolonged and continuous stimulation, LCE fibrous actuators demonstrated actuation stability. Applying a voltage of 2.2, the LCE fiber attained its maximum actuation strain of 46.5%. After 2 hours (1800 s), there was almost no change in the actuating strain. After 24 hours (86400 s), the actuating strain of LCE decreased from 46.5% to 38.9%, and the creep change was approximately 14.2%.

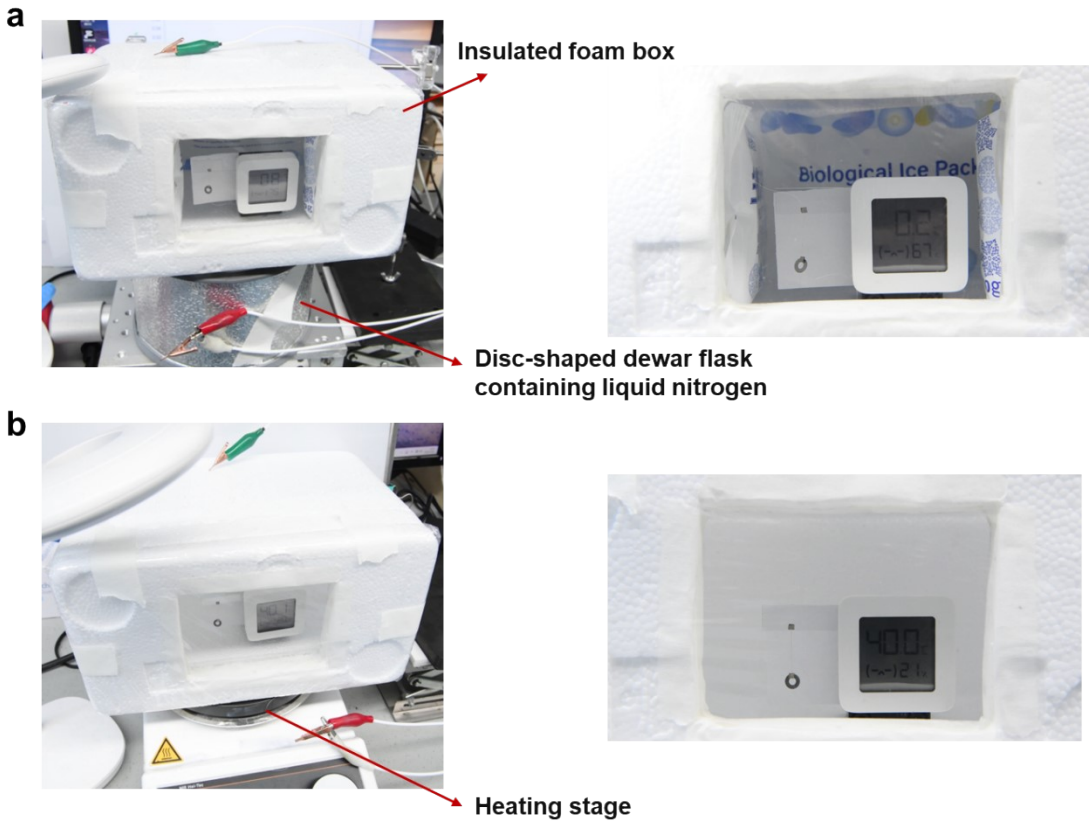

Figure S27. The experimental setup for testing the influence of environmental temperature on the actuation performance of LCE fibers.

The actuation behavior of LCE fibers under 0±1℃, 25±1℃, and 40±1℃ was tested. The low-temperature environment was obtained by putting an insulated foam box containing ice packs on a disc-shaped dewar flask, which was filled with liquid nitrogen (Figure S22a). The high-temperature environment was obtained by putting an insulated foam box on a heating stage at 60 ℃ (Figure S22b). The insulated foam box was sealed with plastic cling film, and two tiny holes were left for silver wires to pass through. Every sample was tested after the system temperature had stabilized for 5 minutes. The laboratory was kept at room temperature throughout the process.

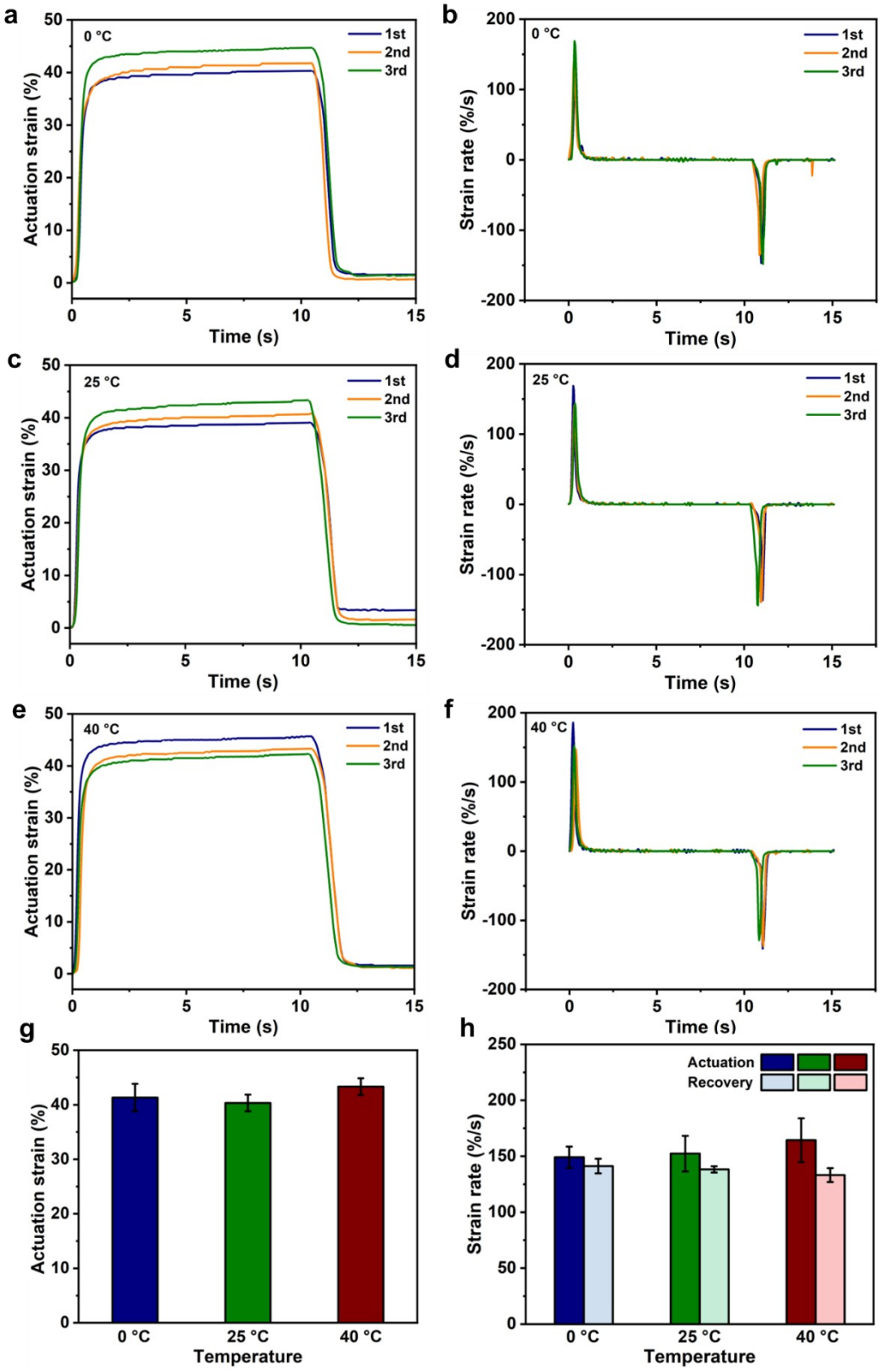

Figure S28. Actuation strain a) and strain rate b) of LCE fibers under 0±1℃. Actuation strain c) and strain rate d) of LCE fibers under 25±1℃. Actuation strain e) and strain rate f) of LCE fibers under 40±1℃. g) Actuation strain of LCE fibers under different environmental temperatures. h)

Strain rate of LCE fibers under different environmental temperatures. All the LCE fibers were actuated by applying a voltage of 2.2 V for 10 s.

The actuation strains of LCE fibrous actuators at different environmental temperatures are close. At 40 ℃, the actuation strain rate is greater, and this is attributed to the time required for LCE fibrous actuators to heat up to the phase transition temperature being shortened. The recovery strain rate increases when the environmental temperature is lower, because a lower environmental temperature is conducive to heat dissipation.

Overall, however, the influence of environmental temperature on the actuation behavior of LCE fibrous actuators is not significant. This is because both air and LCE are poor thermal conductive materials. In the air, the actuation of LCE fibrous actuators mainly relies on the concentrated heating of the Au layer and the thermal conduction of the fibers themselves. If the LCE fibrous actuators are placed in water, the influence of temperature on actuation behaviors would be more obvious.[9]

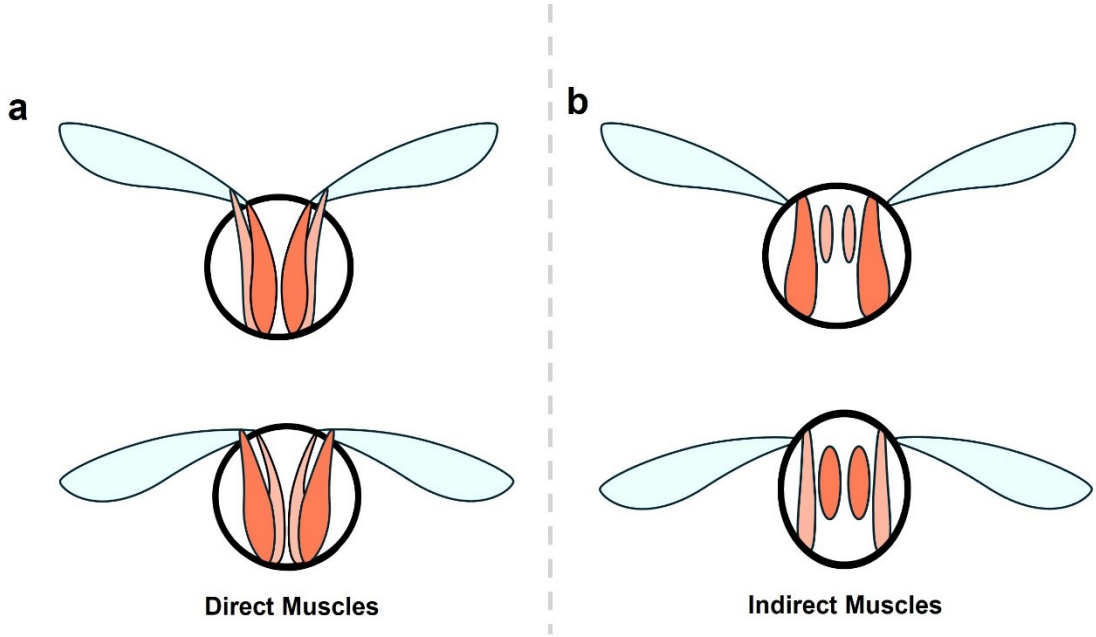

Figure S29. a) Dragonflies control their wings through direct flight muscles. When flying, they can separately control the movement of each wing. Adapted with permission.[10] Copyright 2018 Elsevier. b) Flies, bees, and other insects use the indirect flight muscles of the chest to control their wings to fly. By utilizing expansion and contraction of the chest, they can only control the flapping of a pair of wings simultaneously, but not separately. Adapted with permission.[11] Copyright 2012 Springer Nature.

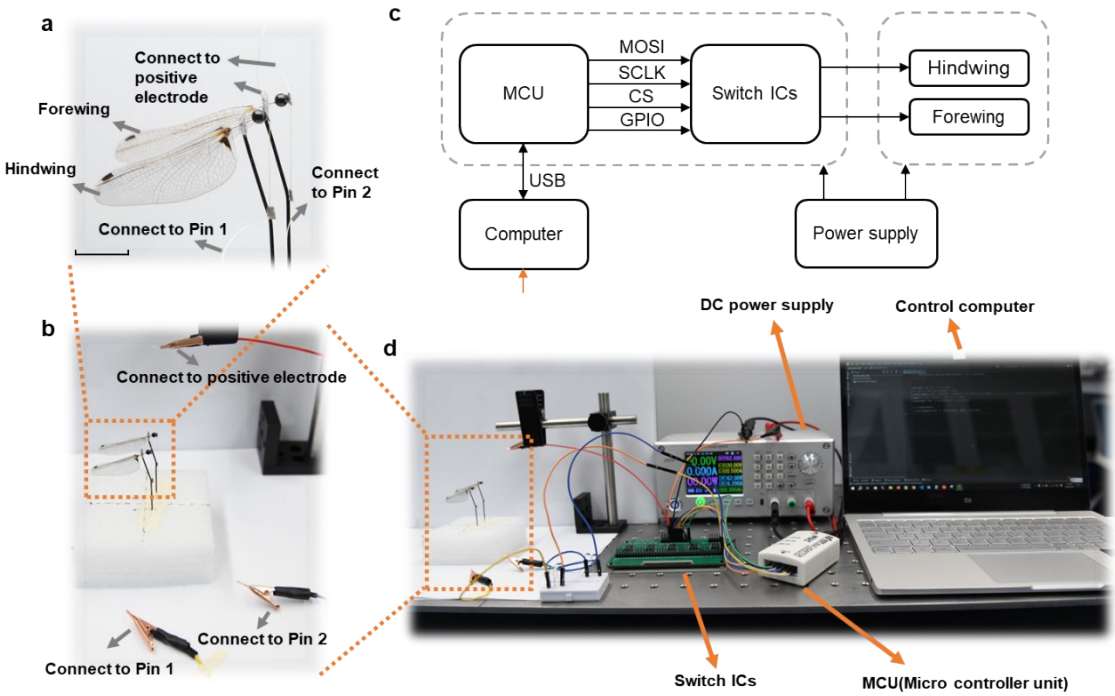

Figure S30. a) The device simulating the flapping-wing control of a dragonfly. Scale bar: 1cm. b) Schematic diagram of the connection of the device and the circuit. c) The control circuitry and d) schematic diagram of the whole application. The LCE fibrous actuators could be driven by power switch ICs MC33996EK (NXP Semiconductors, Netherlands). Power Switch ICs communicate via Serial Peripheral Interface (SPI) to USB2XXX Bus Adapter (UTA0301, TOOMOSS), which communicates with the computer through USB.

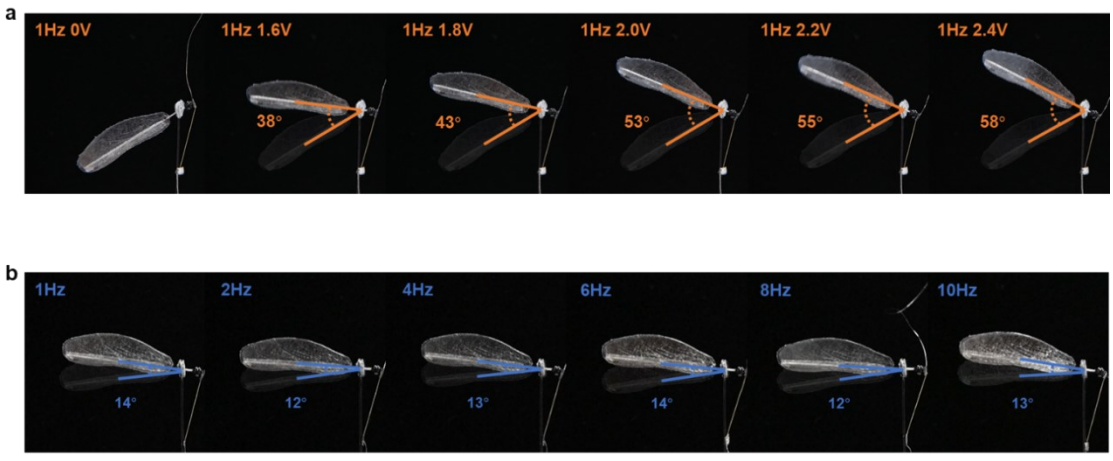

Figure S31. The wings flapped a) at the same frequency but with different amplitudes and b) at the same amplitudes but with different frequencies controlled by a circuit.

1 Z. Hu, Y. Li and J. A. Lv, *Nat. Commun.*, 2021, ***12***, 3211.
2 W. Hou, J. Wang and J.-a. Lv, *Adv. Mater.*, 2023, ***35***, e2211800.
3 J. D. W. Madden, N. A. Vandesteeg, P. A. Anquetil, P. G. A. Madden, A. Takshi, R. Z. Pytel, S. R. Lafontaine, P. A. Wieringa and I. W. Hunter, *IEEE J. Ocean. Eng.*, 2004, ***29***, 706-728.
4 Y. Yu, L. Li, E. Liu, X. Han, J. Wang, Y.-X. Xie and C. Lu, *Carbon*, 2022, ***187***, 97-107.
5 J. Sun, Y. Wang, W. Liao and Z. Yang, *Small*, 2021, ***17***, 2103700.
6 Q. He, Z. Wang, Y. Wang, Z. Wang, C. Li, R. Annapooranan, J. Zeng, R. Chen and S. Cai, *Sci. Robot.*, 2021, ***6***, eabi9704
7 C. Zhu, Y. Zhang, G. He, Y. Shi, Y. Wu, Y. Yu and X. Liu, *Adv. Funct. Mater.*, 2024, ***35***, 2413845.
8 Y. Wang, Q. He, Z. Wang, S. Zhang, C. Li, Z. Wang, Y.-L. Park and S. Cai, *Adv. Mater.*, 2023, ***35***, e2211283.
9 W. Chen, S. Yang, C. Zhu, Y. Cheng, Y. Shi, C. Yu and K. Liu, *Adv. Mater.*, 2025, 2503777.
10 F. Bäumler, S. N. Gorb and S. Büsse, *Arthropod. Struct. Dev*, 2018, ***47***, 430-441.
11 K. Meng, W. Zhang, W. Chen, H. Li, P. Chi, C. Zou, X. Wu, F. Cui, W. Liu and J. Chen, *Microsyst. Technol.*, 2012, ***18***, 127-136.